scientific reports

Check for updates

OPEN

A low cost magnetic biochar manufactured solely from solid wastes by one-step pyrolysis for removal of tetracycline

Xiaohui Zhao✉, Zi Liao, Qingrui Zhao, Mingli Yang, Dongyang Li, Ke Zhang, Xiaodan Wang, Hongpei Zhang & Binguo Zheng✉

Water remediation of toxic chemicals using effective absorbents has received considerable attention recently. In the present study, using peanut shell and red mud as raw materials, a low-cost magnetic biochar (MBC) was prepared via a one-step pyrolysis method, without any chemical input or wastewater discharge, for tetracycline (TC) removal from water. Material characterization and batch processing experiments were conducted to investigate the material properties and environmental factors affecting adsorption performance. The adsorption mechanism of MBC on TC was revealed through adsorption isotherms, adsorption kinetics and thermodynamics analyses. The results show that the MBC material with developed pore structure and rich functional groups is uniformly loaded with nano-Fe_3O_4 particles, and its maximum adsorption capacity of TC reaches 87.39 mg/g, and can be separated from water within 30 s. The simulated removal experiments of MBC demonstrate its promising applications for the removal of various pollutants, such as antibiotics, heavy metals and dyes in real water systems. A regeneration study revealed the high reusability (> 70%) and acceptable stability of MBC even after five cycles. Moreover, the one-step pyrolysis method exhibited good generality for manufacturing MBC from different biomass and significantly reduced cost.

Keywords Peanut shell, Red mud, Magnetic biochar, Tetracycline, Adsorption

Tetracyclines (TCs), a class of antibiotics that can treat a wide range of bacterial infections, including those caused by rickettsial, mycoplasma, chlamydia, and spirochetes, as well as some parasitic diseases, have long been used continuously in the healthcare and aquaculture industries, making them the second most widely used antibiotics in the world[1–3]. TCs have good hydrophilicity and exhibit strong resistance mechanism against up to 130 species of bacteria[4]. As the most commonly used member of the TC class of antibiotics, tetracycline (TC) enters water bodies through human and animal excretion in the form of sewage, feces, and sludge. The input of TC into the water environment also comes from undegraded drug residues in medical wastewater[5], the direct addition of TC in aquaculture, resulting in water residues[6]. the unconsumed drugs enter the treatment plant through the sewage system, but due to the insufficient removal of refractory compounds by the treatment process, they are continuously discharged into the aquatic environment[7].It has been reported that TC concentrations in polluted water have reached mg/L levels[8,9]. Hence, eliminating TC from aqueous solutions is very urgent to reduce its potential risks to humans and the environment.

Magnetic biochar (MBC), as a magnetic separable adsorbent with developed pore structure and abundant surface functional groups, has been used to remove various pollutants from aqueous solutions. In recent years, researchers have successfully prepared MBC for TC removal via various methods, including hydrothermal carbonization, impregnation-pyrolysis, chemical co-precipitation, and ball milling[10–13]. Hang[10] accelerated the hydrothermal carbonization process by adding K_2FeO_4 at 300 °C, and the prepared MBC had strong adsorption capacity for TC (1245.43 mg/g). Using peanut shell and commercial iron salts ($FeCl_3$ and $FeSO_4$) as raw materials, MBC with an adsorption rate of over 85% for TC was prepared via a chemical co-precipitation method, and its maximum adsorption capacity was 71.43 mg/g[12]. Tang[14] prepared MBC by ball milling with bagasse, $FeCl_3$ and $AlCl_3$ as raw materials, and the adsorption capacity of TC in 298 K water reached 116.6 mg/g. Although such progress has been made, the preparation of MBC is still limited by complicated methods, high cost and large amount of wastewater.

School of Civil and Environmental Engineering, Zhengzhou University of Aeronautics, Zhengzhou 450046, China. ✉email: xiaohuizhao@zua.edu.cn; guobinzheng@126.com

One-step pyrolysis has become the most promising method for the preparation of MBC, which only needs to pyrolysis biomass and magnetic precursors at high temperatures in different atmospheres. By pyrolyzing a mixture of corn cob, ferric chloride, CH_3COOK and $C_3H_6N_6$ in a tube furnace at 800 for 1 h, Deng et al.[15] prepared a magnetic biochar with an impressive tetracycline TC adsorption capacity of 764.35 mg/g. Hu et al.[16] synthesized a magnetic biochar using sludge and zero-valent iron as raw materials. The material was pyrolyzed in a muffle furnace at 500 °C for 2.5 h and exhibited a TC adsorption capacity of 81.04 mg/g. Using Fe-rich solid waste as magnetic precursors, instead of commercial iron salts (e.g. $FeCl_3$, $FeSO_4$), can help reduce MBC costs, lower carbon emissions, and achieve resource recycling[17]. Zhou et al. used steel plant water treatment sludge as the raw material to prepare an iron-rich magnetic biochar by pyrolysis at 450 °C for 2 h under N_2 in a tube furnace, which not only had a high adsorption capacity of TC (240.38 mg/g), but also effectively controlled the dissolution of heavy metals [18].

Red mud (RM) is a grayish-red or dark red residue emitted in the production process of alumina, which is strongly alkaline and rich in Fe (Fe_2O_3: 5–60% by wt.), and has a huge emission[19]. According to statistical estimates, the global output of alumina in 2022 is 142.23 million tons, and the emission of RM is close to 200 million tons[20]. At present, the disposal method for RM is still dominated by open-air storage of tailing ponds, which not only occupies a large amount of valuable land, but also poses hidden dangers, such as soil pollution, groundwater pollution, and dam break. These huge RM tailings ponds have caused a number of world-famous disasters, such as the dam break accident in Ajka, Hungary in 2010, and Belem, Para, Brazil in 2018[21,22]. Hence, there is an urgent need for promoting the safe treatment and reuse of RM. Loebsack[23] used RM and Canadian pine as raw materials in CO_2 atmosphere and pyrolysis at 800 °C for 3 h to produce MBC. The material has good magnetic properties and the adsorption capacity of acetaminophen reaches 32.8 mg/g. Ahmed[24] pyrolyzed RM and rice straw at 700 °C, and the removal rate of Pb^{2+} reached 98.17%. Yang[25] pyrolysis RM and walnut shells in N_2 atmosphere to produce MBC, and the adsorption capacity of phosphorus reached 15.48 mg/g.

Peanuts play a significant role as an oil crop. In 2019, the global peanut production reached 48.8 million tons, with a corresponding peanut shell production of 15 million tons[26]. Unfortunately, except for a small portion used as feed or chemical raw materials, the majority of peanut shells are either directly burned or discarded in farmland, leading to environmental pollution and resource waste. Peanut shells are known to consist of microfibers rich in cellulose and hemicellulose, with a low ash content[27]. In recent years, peanut shell has been utilized as a substrate for the synthesis of various magnetic biochars[28–30]. However, there are few reports on the use of peanut shell composited with red mud to prepare adsorption materials for antibiotics removal. Xu et al.[31] prepared MMBC materials by pyrolyzing nitric acid-modified red mud composited with peanut shells. This method was found to enhance the surface pore structure and remove undesirable elements from RM. Deng et al.[32] prepared an MRP catalyst using peanut shells and acid-modified red mud as raw materials through a co-pyrolysis method. In a batch/fixed-bed reactor system, the catalyst achieved highly efficient degradation of pollutants in dye wastewater, with Fe^{2+} and oxygen-containing functional groups playing a dominant role in the catalytic process.The preparation of magnetic biochars often involves the addition of pore-forming agents, strong oxidants, strong acids, and strong bases to obtain a developed pore structure and abundant surface functional groups. This approach commonly results in the generation of wastewater, with less attention paid to the environmental friendliness of the preparation method. Additionally, there are shortcomings in the calculation of preparation costs, which may not fully account for the entire production process.

Herein, a low-cost MBC was prepared by a one-step pyrolysis method using RM and peanut shell. The effects of various parameters, such as dosage of MBC, initial concentration, pH, temperature and coexisting ions of TC solution on TC adsorption were investigated. The removal performance of different types of pollutants in real water was evaluated, and the preparation cost was calculated considering each step of the process, including labor and capital investment. The adsorption mechanism of MBC on TC was discussed through adsorption kinetics, isotherm, and thermodynamic analyses, as well as material characterization before and after adsorption process. The universality of the preparation method for different biomass materials was analyzed, which expands the horizon for the recycling of bulk solid waste resources and the preparation of green low-carbon water treatment materials.

Results and discussion

Characterization

Figure 1 shows the micromorphology of MBC. As seen in Fig. 1a, the MBC surface exhibits numerous pores, which creates more adsorption channels and increases the specific surface area of the material. This porous structure is favorable for the surface adsorption and internal diffusion of TC molecules within MBC materials. Figure 1b shows that white nanoparticles are distributed on the surface of the material. The results of energy dispersion spectroscopy (EDS) in Fig. 1c reveal that Fe mass ratio is 27.02%. Figure 1d, e shows the mapping diagram of EDS elements. The large number and wide distribution of light spots in the picture indicate that Fe elements are successfully loaded on the surface of MBC and distributed evenly.

The N_2 adsorption–desorption isotherm of MBC is shown in Fig. 2. The N_2 adsorption and desorption isotherms of MBC exhibit a Type IV pattern, indicating that the adsorption material is predominately mesoporous. The presence of a large number of mesoporous materials can promote the diffusion of TC into the pores of MBC materials, thereby improving the adsorption performance. The H4 type hysteresis loop observed at relative pressures between 0.1 and 0.9 indicates that the adsorption material has capillary condensation in the higher pressure range and contains a certain number of microporous structures[33]. The pore size distribution curve and Table 1 further reveal that the MBC material has a rich porous structure, consisting of both mesoporous and microporous, and the diameter is basically below 50 nm, which is consistent with the microstructure characteristics observed in the SEM analysis.

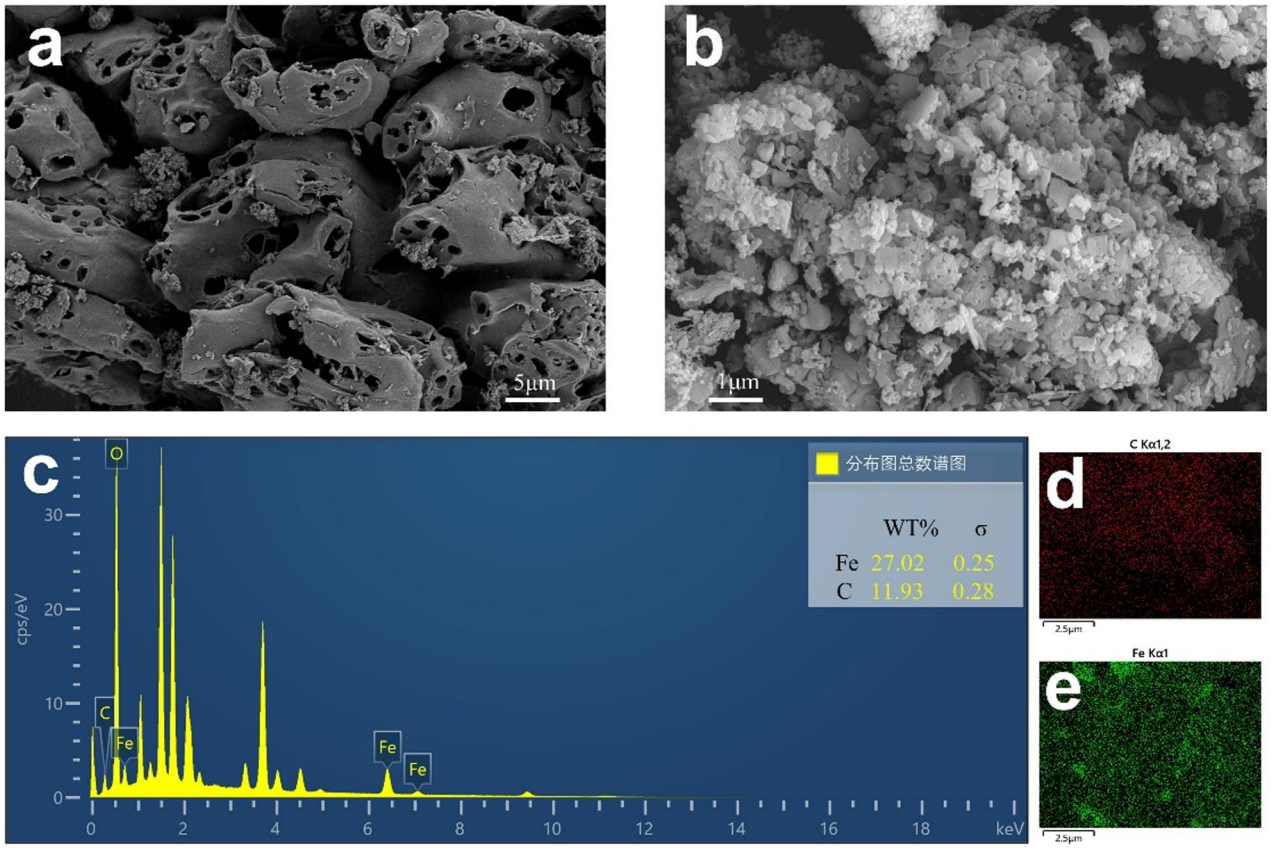

Fig. 1. SEM images of MBC (**a**, **b**); Elemental analysis of MBC (**c**, **d**, **e**).

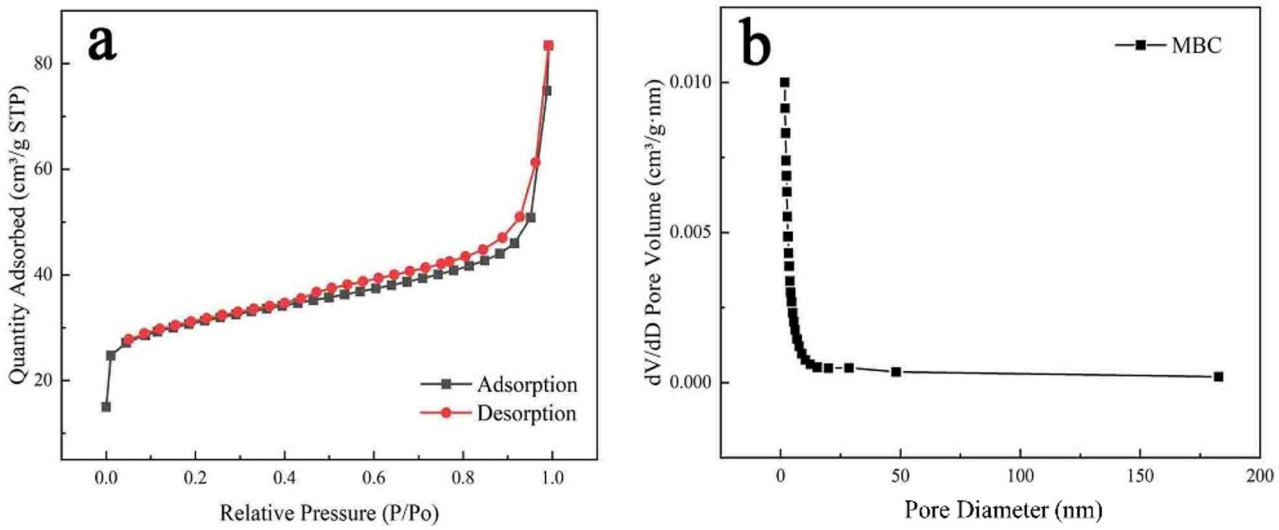

Fig. 2. (**a**) N_2 adsorption–desorption isotherm of MBC; (**b**) Pore size distribution of MBC.

Material	BET surface area (m^2/g)	Total pore volume ($10^{-3}cm^3/g$)	Average aperture (nm)
MBC	113.75	0.13	4.54

Table 1. Pore structure parameters of MBC.

The XRD pattern is shown in Fig. 3. As can be seen from the graph, there are several sharp peaks at 2θ = 34.8°, 36.9°, 38.9°, 42.0°, 51.1°, 56.1°, 68.0° and 74.1°, correspond to the (220), (311), (222), (400), (422), (511), (440) and (533) crystal faces, respectively. These diffraction peaks are characteristic of the magnetite (Fe_3O_4) (JCPDS, No. 88–0866). The high peak height and strong signal response observed in the XRD pattern confirm the existence of Fe_3O_4 crystals in the prepared MBC material[34]. The characteristic peak at 2θ = 16.6°and 45.2° correspond to the presence of Al_2O_3[35]. The characteristic peaks at 25.1°, 32.1°, 35.7°, and 63.9° correspond to Fe_2O_3[36]. Additionally, the peaks at 22.6°, 27.2°, 28.8°, and 70.1° correspond to $AlNaO_4Si$, SiO_2, Ca_2SiO_4, and $MgCO_3$, respectively[37]. The formation of the above substances is likely related to the presence of red mud in the raw materials.

As shown in Fig. 4, the peak at 3430–3440 cm^{-1} can be attributed to the stretching vibration of O–H groups on the surface of MBC sample, indicating the presence of a large number of carboxyl and hydroxyl groups on the surface of MBC. The peaks observed at 1330–1350 cm^{-1}, 993–996 cm^{-1}, and 773–780 cm^{-1} correspond to the C = C stretching vibration, C–O stretching vibration, and C–H stretching vibration, respectively—all of which are characteristic signatures of aromatic hydrocarbon structures[38,39]. The wide peaks observed around 539–541 cm^{-1} are attributed to the tensile vibration of the Fe–O bond, corroborating the results of XRD and indicating the presence of ferrite compounds in the prepared MBC material[40,41]. It is worth noting that the appearance of the above characteristic peaks indicates that a variety of functional groups including carboxyl group, hydroxyl group, carbonyl group and Fe–O bond are formed on the surface of magnetic biochar adsorbents, creating conditions for chemisorption.

As can be seen from the total spectrum of Fig. 5a, the characteristic peaks of C, N, O and Fe were identified on the surface of MBC, which were located at 285.2, 399.85, 533.26 and 711.29 eV, respectively. This is consistent with the XPS characterization results reported by Zhang et al.[38]. As can be seen from the spectra of C 1 s (Fig. 5b) and O 1 s (Fig. 5d), oxygen-containing functional groups such as C–O, C = O, and O–C = O exist on the surface of MBC, which can facilitate the chemisorption with TC through π-π and hydrogen bonding[42,43].The appearance of the characteristic peak of Fe (Fig. 5f) further corroborates the findings from the SEM, FT-IR and XRD, indicating the successful loading of iron oxides in MBC.

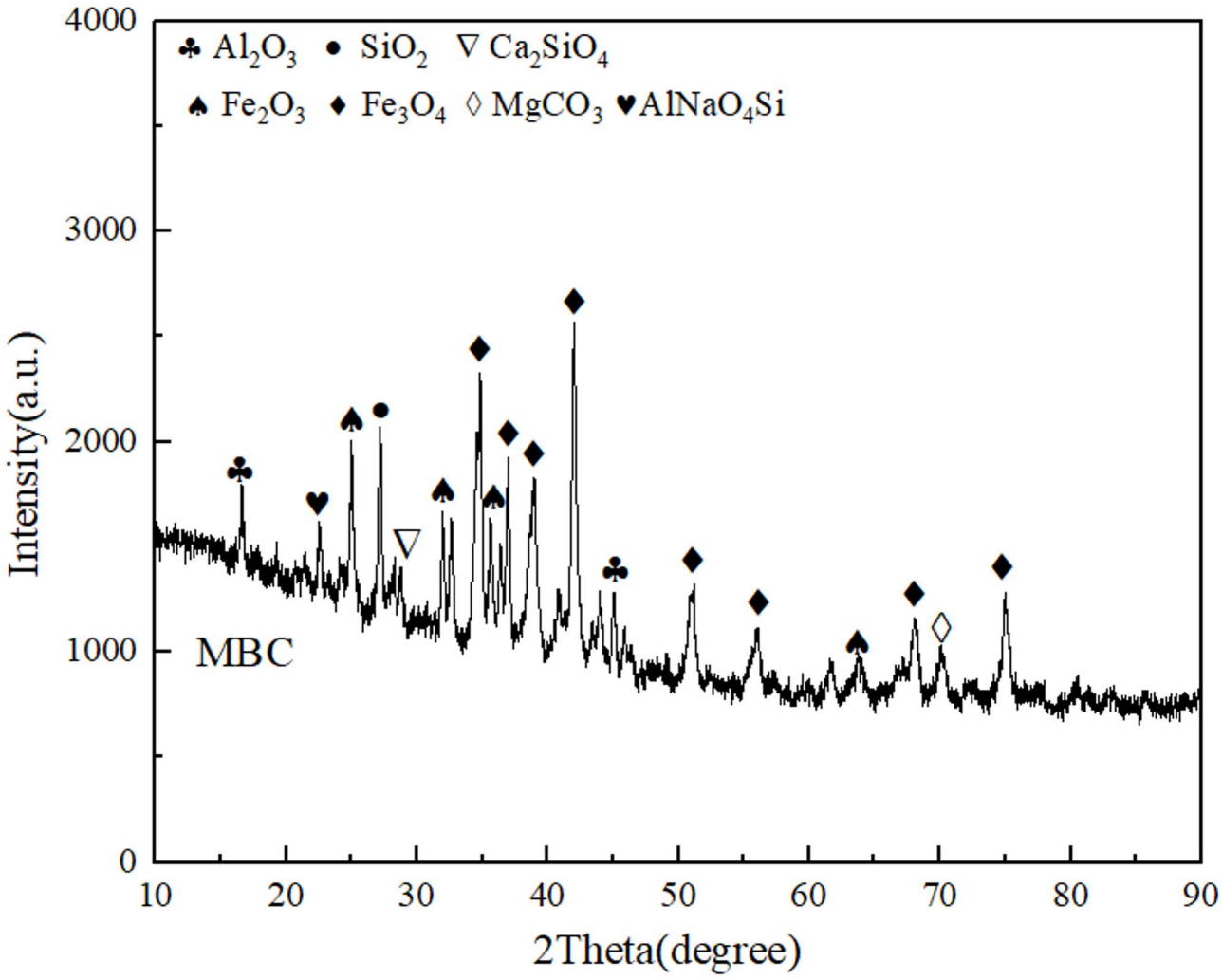

Fig. 3. XRD spectra of MBC.

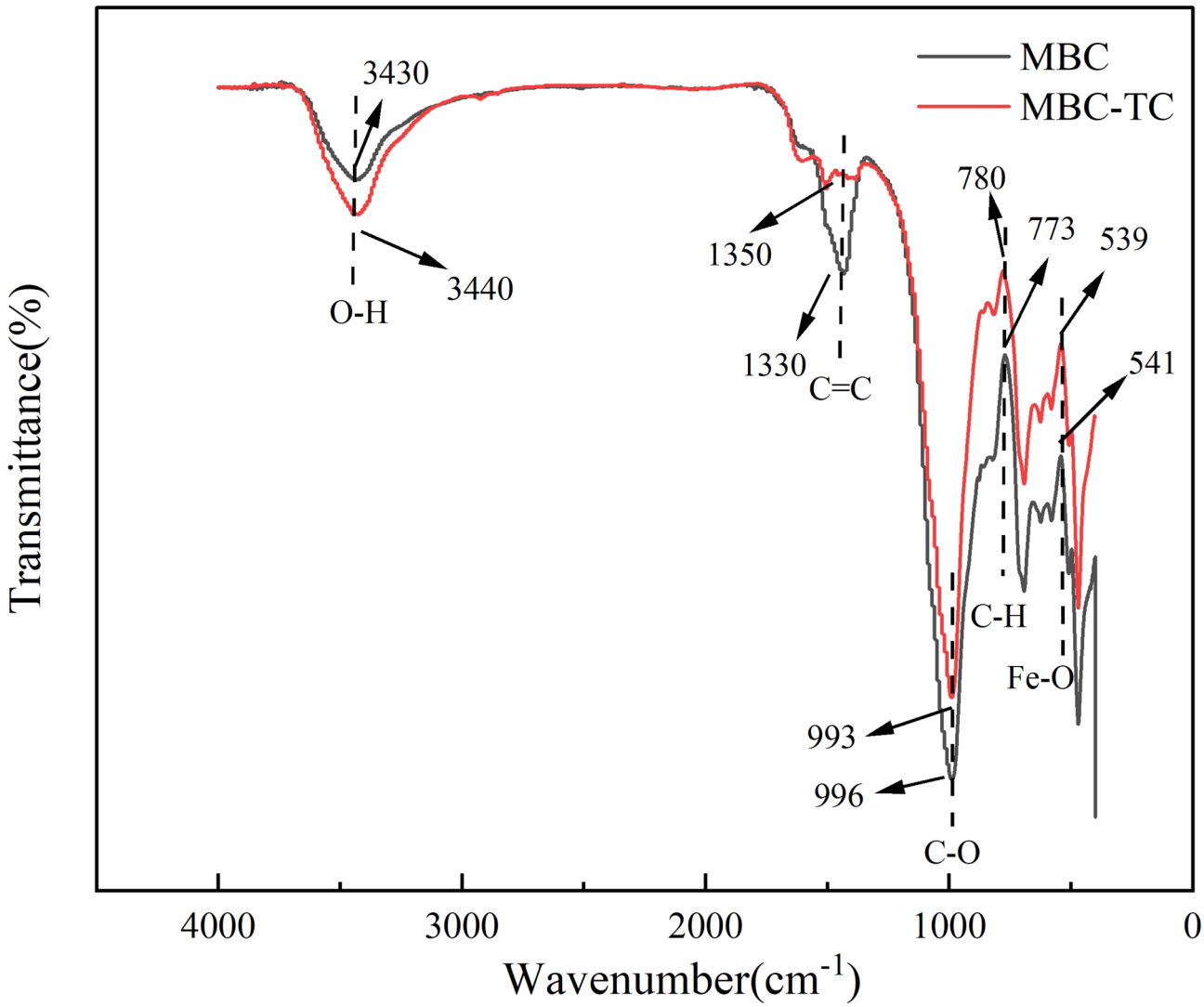

Fig. 4. FT-IR spectra of MBC, MBC-TC.

The hysteresis loop of MBC and its related magnetic parameters are shown in Fig. 5h. The magnetization of MBC increases with the applied magnetic field and reaches saturation, showing typical ferromagnetic characteristics with an intensity value of 7.21 emu/g. Under the action of 1.2 T magnetic rod, MBC can be separated from MG solution within 30 s, indicating that the material can quickly achieve solid–liquid separation.

Analysis of influencing factors on TC removal

Under the conditions of initial concentration of TC solution 30 mg/L, T = 20 °C and pH = 7, the effects of different doses of MBC (10–80 mg) on the adsorption performance were investigated, as shown in Fig. 6. The adsorption efficiency increased gradually as the dosage of MBC adsorbent increased from 10 to 30 mg, reaching a maximum of 92.6% at the dosage of 30 mg. Moreover, in the range of MBC dosage from 30 to 70 mg, the increase of adsorption efficiency was negligible. This can be attributed to the fact that with the increase of the adsorbent dosage, the active sites continue to increase, but eventually reaches a point where there is an excess of active sites, and the utilization rate of active sites on the surface of the material is reduced, resulting in waste of materials. Therefore, 30 mg MBC dosage was used in subsequent experiments.

Under the conditions of TC dosage = 30 mg, T = 20 °C and pH = 7, the effects of different initial concentrations (10–100 mg/L) on the adsorption performance were investigated, as shown in Fig. 7. As the initial concentration of TC increased from 10 to 100 mg/L, the adsorption capacity of MBC increased from 15.1 to 81.7 mg/g. In terms of adsorption rate, when the initial concentration of TC was increased from 10 to 30 mg/L, the adsorption rate of TC remained relatively unchanged. However, when the initial TC concentration exceeds 30 mg/L, the adsorption rate begins to decline sharply. At the highest initial concentration of 100 mg/L, the adsorption rate dropped to 47.3%. This can be attributed to the fact that at higher initial TC concentrations, the adsorbent material does not have a sufficient number of available active sites to effectively adsorb the TC molecules in the

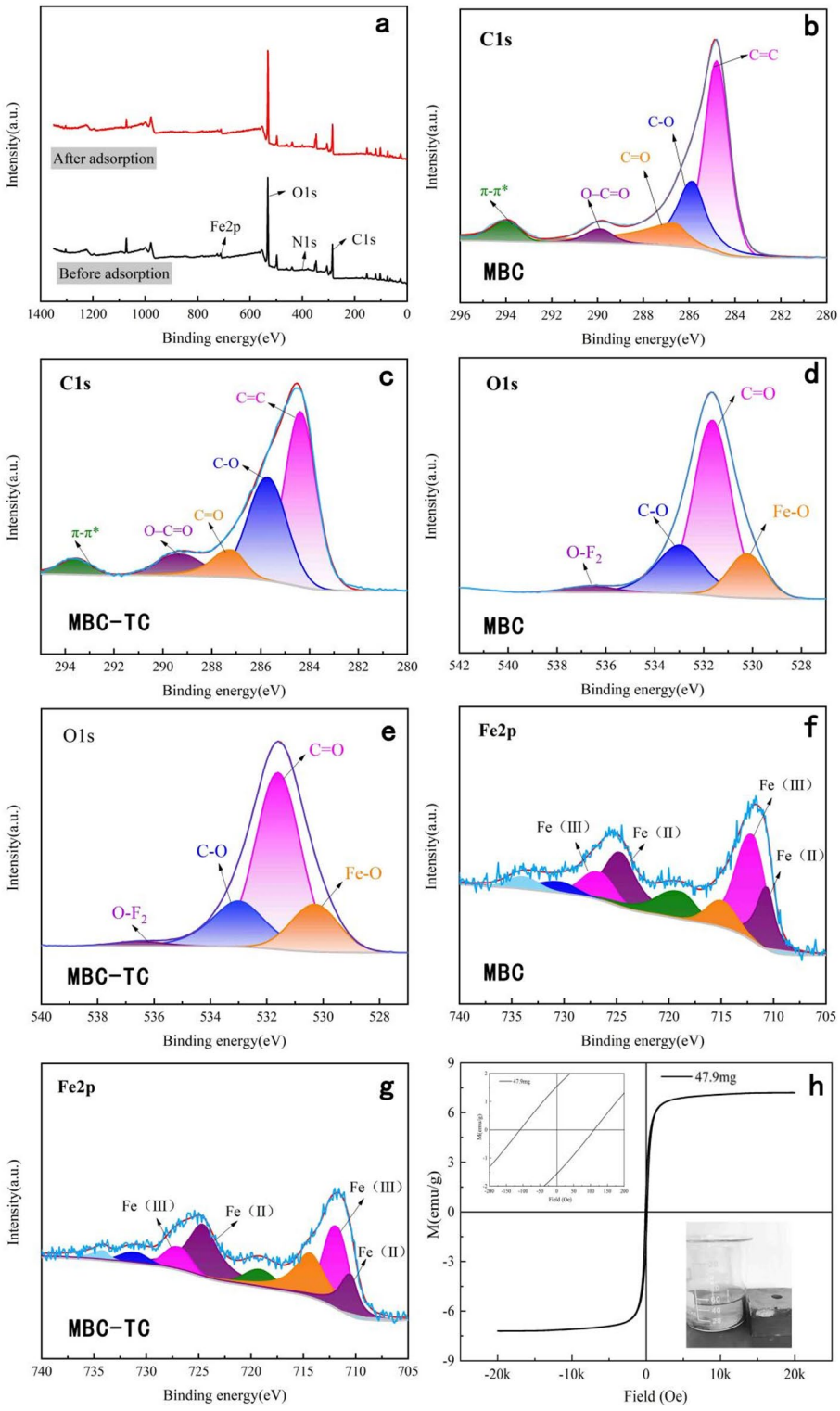

Fig. 5. XPS total spectrum of MBC before and after adsorption (**a**); XPS spectra of MBC C, O, Fe element before and after adsorption (**b**–**g**); solid–liquid separation of MBC (**h**).

solution. Considering the high adsorption rate, the initial concentration of TC in subsequent experiments was set at 30 mg/L.

The pH of the solution is an important factor affecting adsorption. In order to explore the effect of different pH values on the adsorption performance of TC by MBC, the initial pH of TC solution was adjusted to 3, 5, 7, 9 and 11, respectively, and the adsorption experiment was carried out under the conditions of 30 mg MBC dosage, 30 mg/L TC concentration and T = 20 °C. According to the literature[44], TC is an amphoteric compound,

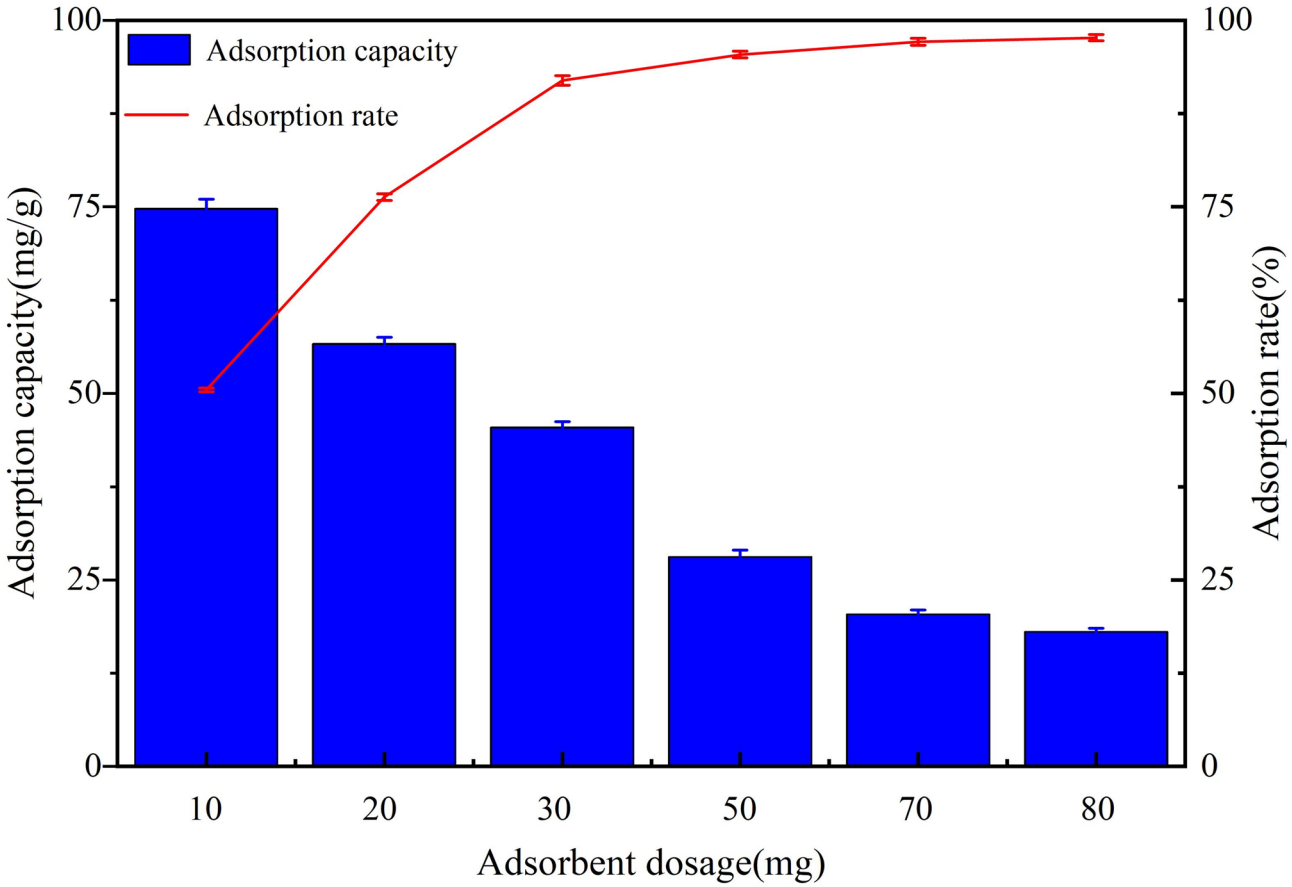

Fig. 6. Effect of different adsorbent dosage on TC removal (TC 30 mg/L, pH = 7, 20 °C).

and the hydrolysis constants of TC are $pK_{a1} = 3.3$, $pK_{a2} = 7.7$ and $pK_{a3} = 9.7$, respectively. When the solution pH is less than 3.3, TC exists predominantly in a cationic state (TCH^{3+}). In the pH range of 3.3–7.7, TC is mainly in a zwitterionic form (TCH_2). When the pH value is greater than 7.7, TC is anionic (TCH^- and TC^{2-}). The zeta potential test results of MBC material are shown in Fig. 8a. The net surface charge of MBC is positive when the solution pH is less than 6.6, and negative when the solution pH is greater than 6.6. As shown in Fig. 8b, MBC has the highest adsorption capacity of TC when pH is 7. In the pH range of 3–7, the adsorption capacity of MBC on TC increases, which can be attributed to the electrostatic attraction of TCH_2 molecules by the positive charge on the surface of MBC. In the pH range of 7–11, the adsorption capacity of MBC to TC decreases,likely due to the existence of electrostatic repulsion between the electronegative charge on the surface of MBC material and the negative ions of TCH^- and TC^{2-}, which prevents the adsorption of TC molecules on the surface of MBC.

MBC materials exhibit relatively stable adsorption performance across a wide pH range (3–11), suggesting their potential for application under various acid–base conditions. The adsorption performance of MBC on TC did not decrease significantly under alkaline conditions, and the adsorption capacity at pH = 11 (42.7 mg/g) was still 93% of that at neutral conditions (46.1 mg/g). Zhang et al.[45] used bagasse, red mud, $C_3H_6N_6$ and $NaHCO_3$ as raw materials to prepare magnetic biochar for TC adsorption via one-step pyrolysis, with pH_{PZC} of 6.7. Their adsorption experiments across different pH conditions showed the best performance at pH 6.58, with the adsorption effect decreasing slightly between pH 7 and 10, but still maintaining an adsorption rate above 90%. Deng et al.[15] used corn cob, $FeCl_3$, $C_3H_6N_6$ and CH_3COOK as raw materials to prepare magnetic biochar by one-step pyrolysis. Zeta potential test revealed that the material surface carries a predominantly positive charge when the pH is less than 6.09, and a predominantly negative charge when the pH exceeds 6.09. The maximum adsorption capacity of magnetic biochar for TC appeared at pH = 5. While the adsorption capacity gradually decreased in alkaline environment, reaching a minimum at pH = 12, it still remained at 83% of the maximum adsorption capacity, indicating that the adsorption performance did not decline sharply.

Under alkaline conditions, the net surface charge of these magnetic biochar materials becomes negative, and TC exists in the form of negative ions (TCH^- and TC^{2-}). This creates a certain degree of electrostatic repulsion between the adsorbent and adsorbate. However, the adsorption performance is not significantly reduced, suggesting that mechanisms other than electrostatic interaction are at play. FT-IR analysis revealed that there were several types of oxygen-containing functional groups on the surface of MBC. These functional groups can participate in hydrogen bonding interactions with the TC molecules. As the pH increases and the negative charge accumulation on the MBC surface intensifies, the charge-assisted hydrogen bonding (CAHB) interactions are further strengthened. This strengthening of CAHB interactions appears to overcome the increased electrostatic

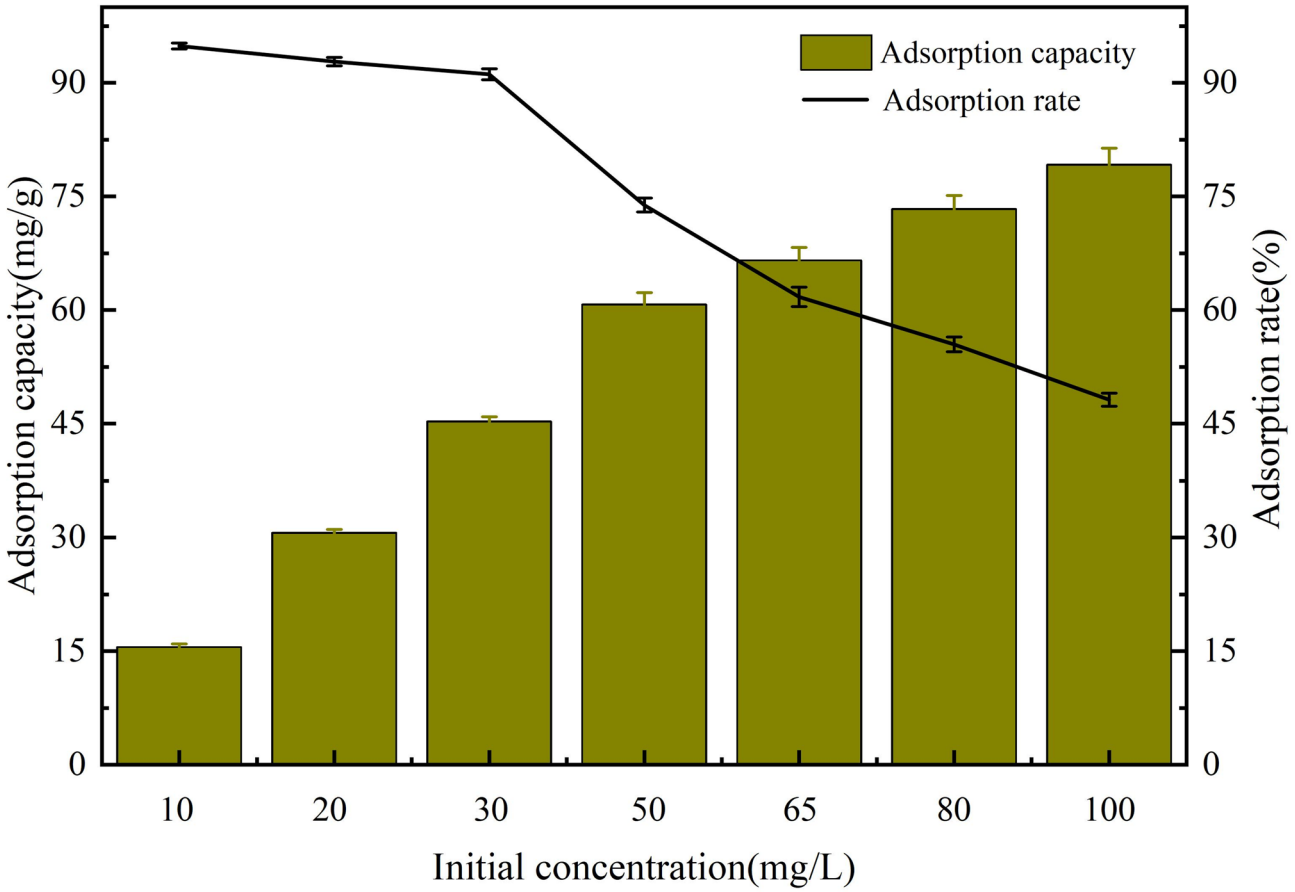

Fig. 7. Effect of different concentrations on TC removal (MBC 30 mg, pH = 7, 20 °C).

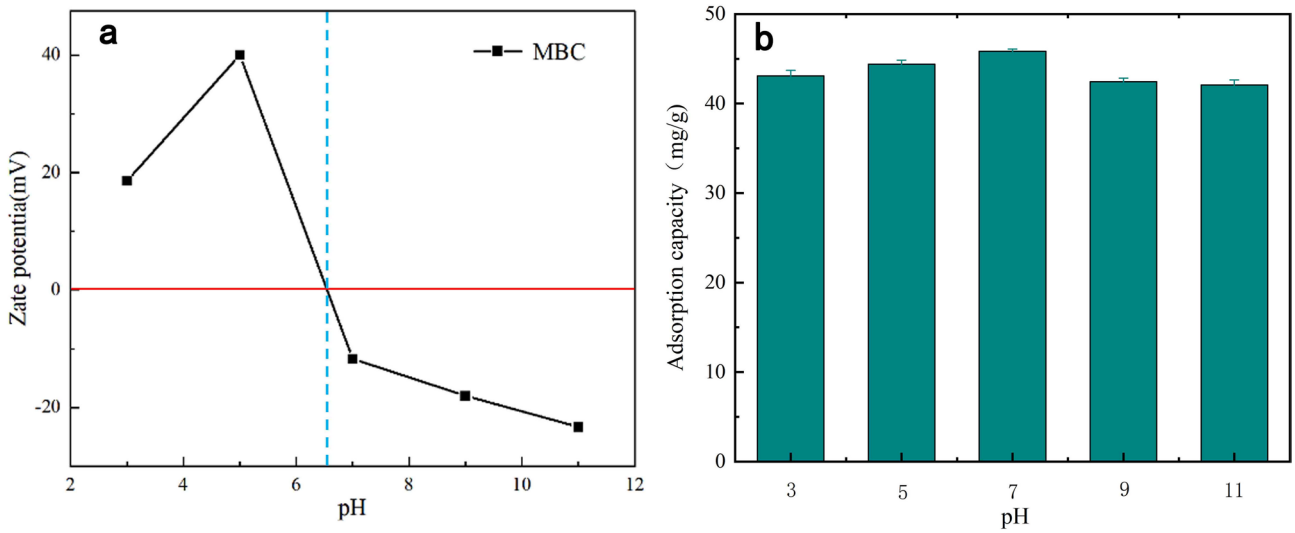

Fig. 8. Zeta potential of MBC material (**a**); Effect of different pH on TC removal (**b**) (MBC 30 mg, TC 30 mg/L, 20 °C).

repulsion, allowing the adsorbent to maintain considerable adsorption capacity for TC even under alkaline conditions[40,46].

In order to investigate the effect of temperature on the removal efficiency, the adsorption properties at 10 °C, 15 °C, 20 °C, 25 °C and 30 °C were investigated under the conditions of 30 mg MBC dosage, 30 mg/L solution concentration and pH = 7. As can be seen from Fig. 9, the adsorption capacity is positively correlated

with temperature. This relationship is particularly pronounced at temperatures below 20 °C, indicating that a rise in temperature is conducive to the adsorption process. This observation is consistent with the results of thermodynamic calculations, which suggest that the adsorption process is endothermic in nature. The increase in temperature can reduce the thickness of the boundary layer around the adsorbent, facilitating the migration of pollutants to the adsorbent in the liquid phase. The high temperature induces the surface of the adsorbent to become homogeneous, thus enhancing the affinity for pollutants. In addition, the rise in temperature can activate more adsorption sites on the adsorbent surface, leading to an increase in the number of active sites, which was conducive to the occurrence of adsorption[16,47,48]. Based on the observed relationship between adsorption capacity and temperature, as well as the consideration of energy efficiency, the use of MBC at a temperature of 20 °C appears to be a reasonable choice for the removal of TC.

The natural water dissolved and accumulated inorganic ions and organic ions under the action of water circulation. Industrial wastewater can also introduce a variety of inorganic ions from raw materials and chemicals used in the production and treatment processes. The co-existing ions in water can have a certain effect on the adsorption of pollutants, so it is necessary to explore the interference of these ions on the adsorption process. Therefore, the interference of inorganic ions (2 and 20 mmol/L) such as NO_3^-, SO_4^{2-}, Cl^-, HCO_3^- and CO_3^{2-} on adsorption was investigated through batch adsorption experiments, and the influence of humic acid (HA, 10 mg/L and 20 mg/L) was explored. At MBC dosage of 30 mg, TC concentration of 30 mg/L, and water temperature of 20 °C, $NaNO_3$, Na_2SO_4, NaCl, $NaHCO_3$ and Na_2CO_3 were added respectively to form corresponding ion concentration solutions to carry out adsorption experiments. It can be seen from Fig. 10 that among the tested inorganic ions, the presence of NO^{3-} and CO_3^{2-} has the greatest influence on the adsorption capacity, especially at higher ionic concentrations. The adsorption capacity decreased from 40 to around 30 mg/g, which may be due to the electrostatic interaction, hydrogen bonding, and coordination, which led to these inorganic ions occupying the adsorption site and thus forming a competitive relationship with TC. As can

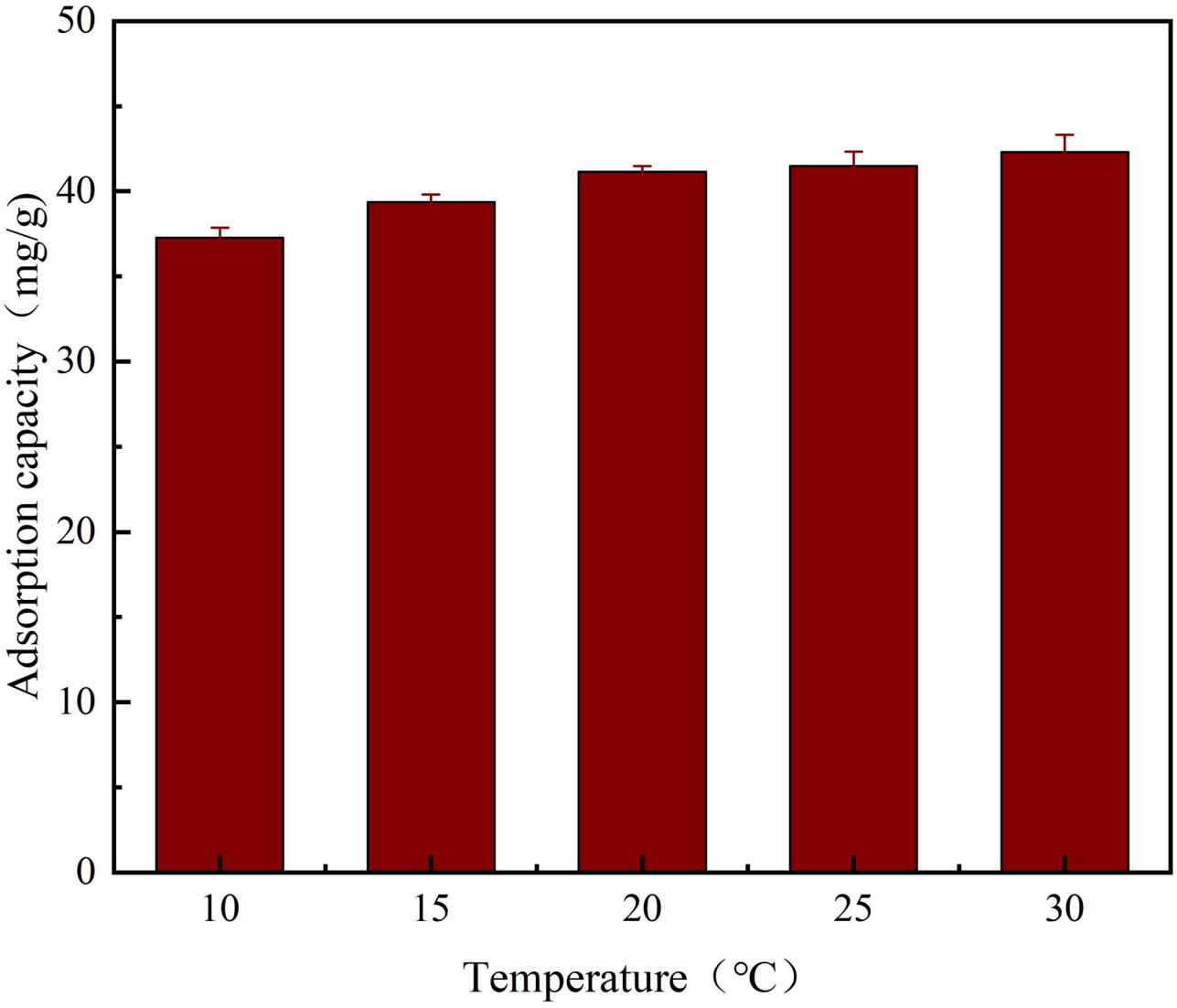

Fig. 9. Effect of different reaction temperatures on TC removal (MBC30 mg, TC30 mg/L, pH = 7).

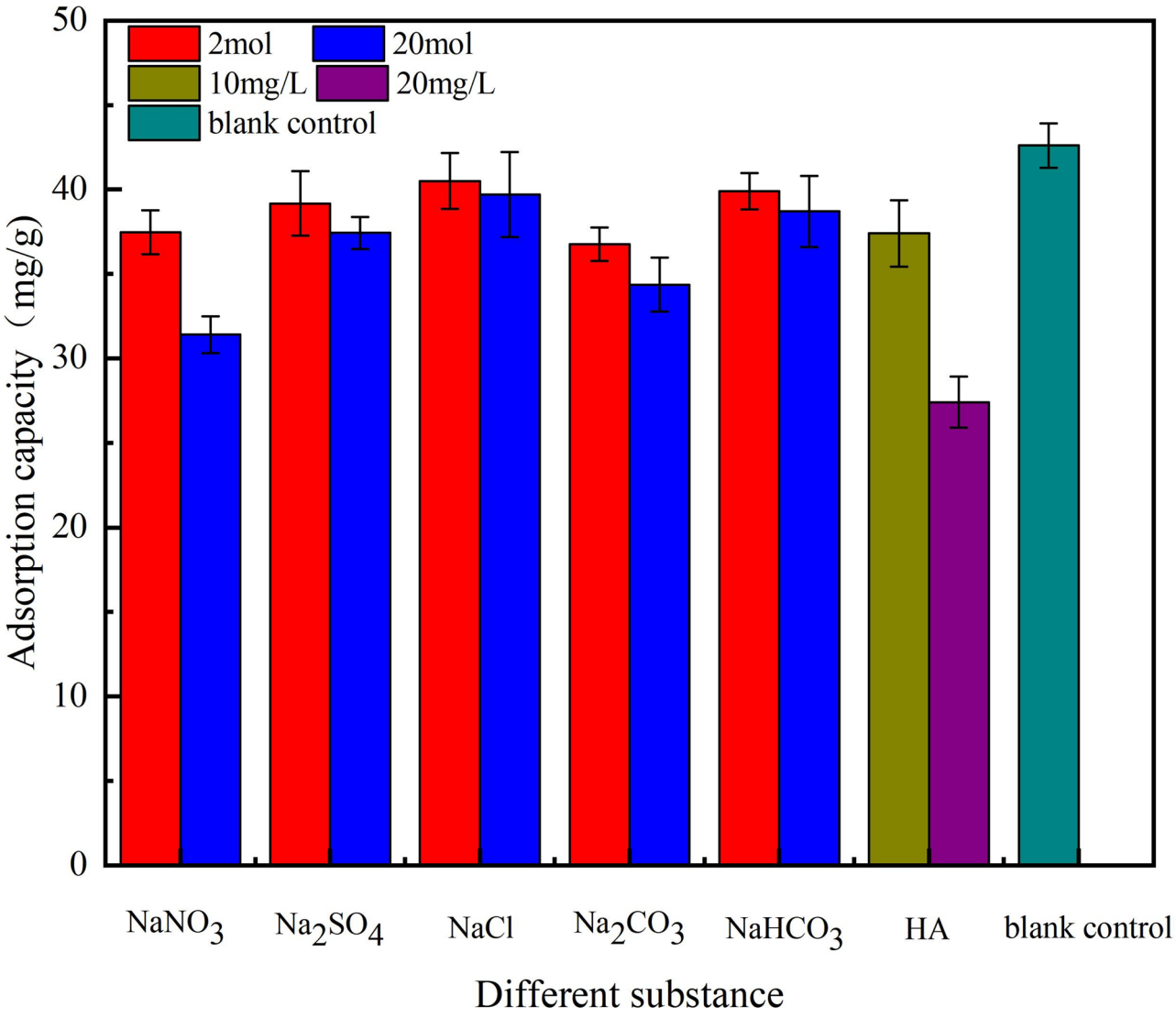

Fig. 10. Effect of coexisting ions on TC removal (MBC 30 mg, TC 30 mg/L, T = 20 °C).

be seen in Fig. 7, with the increase of HA concentration, the adsorption capacity of MBC for TC decreases, and the adsorption capacity drops sharply to below 30 mg/g when HA concentration is 20 mg/L. Ma et al.[40] studied the effect of coexisting ions on the adsorption process of N-doped magnetic biochar TC, and the results showed that the increase of HA concentration limited the adsorption process, which was consistent with the present study. The reduction in adsorption capacity in the presence of HA may be due to the formation of competitive adsorption between HA and TC, or the generation of HA-TC complexes, which can decrease the affinity of MBC towards TC[49].

Reuse performance is an important index for evaluating the application potential of adsorbent technology, as it is not only related to material properties, but also affected by desorption regeneration methods. In this study, the desorption and regeneration experiment of MBC were carried out by ultrasonic regeneration. First, the MBC was separated from the TC solution with a magnet and placed in a tapered bottle with a plug. Then, 100 mL of distilled water was added, and the mixture was subjected to 2 h of ultrasonic treatment to facilitate desorption. After the desorption step, the 0.45 filter membrane was washed 3 times with deionized water in the filter pumping machine and dried in a vacuum drying oven. The removal efficiency after repeated regeneration is shown in Fig. 11. After the first regeneration, the decline in removal rate was significant, but then gradually slowed down. Notably, the adsorption capacity remained above 70% of the original after 5 regeneration cycles, with good reuse.

Removal mechanism of TC in water

The study of adsorption kinetic model is helpful in revealing the adsorption mechanism. Figure 12a displays the results about the impacts of adsorption time on the adsorption capacity of MBC adsorbent, as well as the results of kinetics data fitted by using the Quasi-first-order, Quasi-second-order, and Elovich models. Furthermore, the fitting results of the intraparticle diffusion model are displayed in Fig. 12a. For the fitted model, the square of the

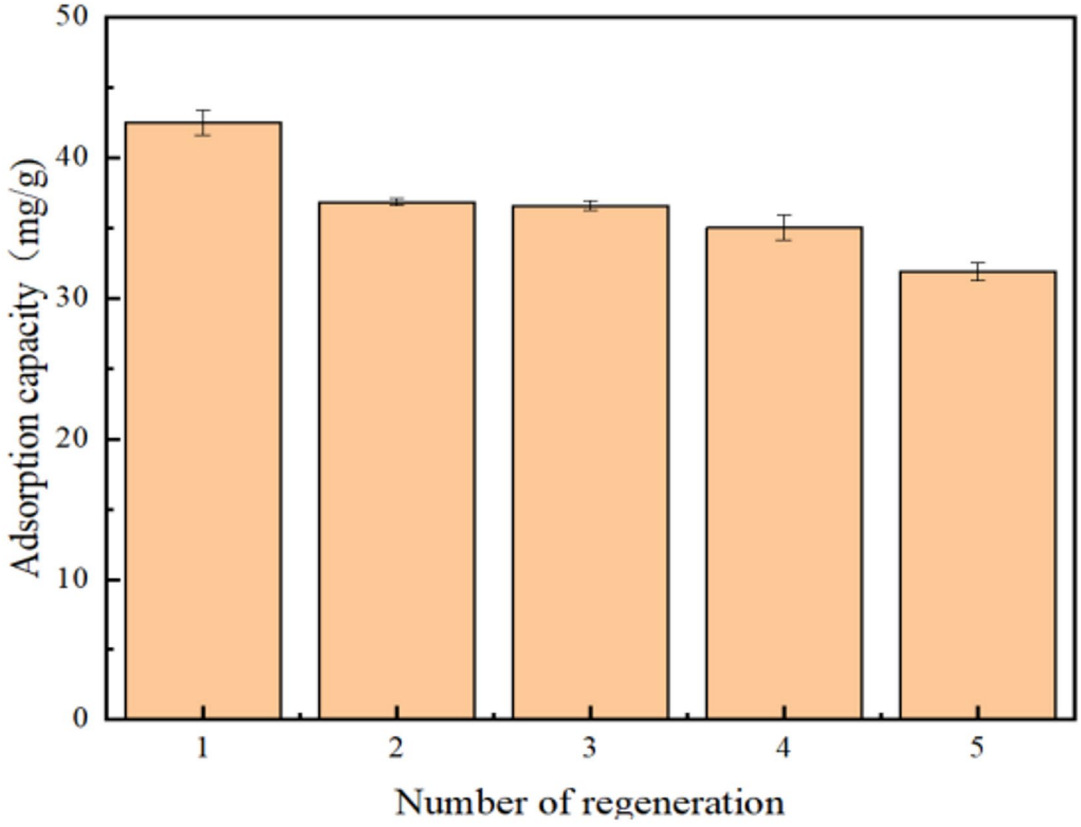

Fig. 11. Performance of repeated use.

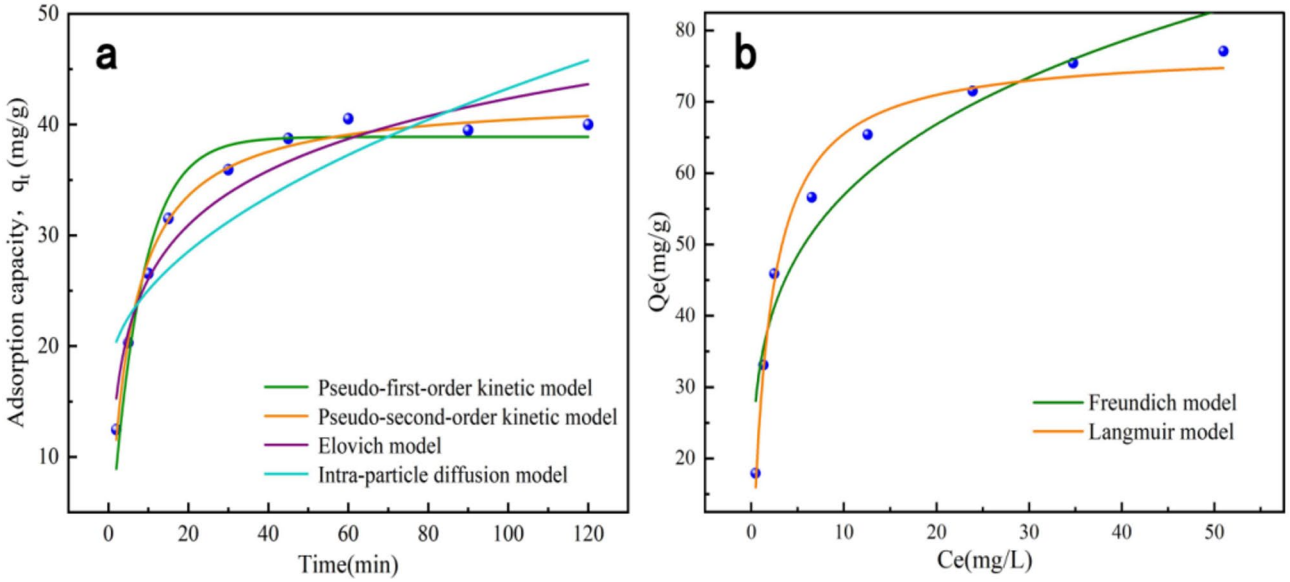

Fig. 12. The fitting curves of kinetic models (**a**) and isotherm models (**b**).

Quasi-first-order model			Quasi-second-order model			Elovich model			Intra-particle diffusion model		
Q_e (mg/g)	K_1	R^2	Q_e (mg/g)	K_2	R^2	a	b	R^2	K_3	C	R^2
38.894	0.13	0.961	42.59	0.004	0.993	26.722	0.14	0.934	2.663	16.632	0.773

Table 2. Parameters of kinetic model for adsorption of TC (TC 30 mg/L, pH = 7, T = 20 °C, MBC 30 mg).

Freundlich model			Langmuir model		
n	K_F	R^2	Q_m(mg/g)	K_L	R^2
4.31	33.393	0.931	87.39	0.551	0.987

Table 3. Isotherm parameters of adsorption of TC by MBC (TC 10–100 mg/L, pH = 7, T = 20 °C, MBC 30 mg).

fitting coefficient (R^2) was used to evaluate the fitting quality. As depicted in Fig. 9, due to the large number of available adsorption sites on the surface of the adsorbent in the initial stage, the amount of TC adsorbed by the material increases rapidly within the first 15 min. Thereafter, the increase in adsorption capacity gradually slows down, and the adsorption equilibrium is achieved at around 60 min. It can be seen from Table 2 that it is more appropriate to use the quasi-second-order kinetic equation to describe the adsorption process of TC by MBC, with an R^2 of 0.993. The fitting results of Elovich model ($R^2 = 0.934$) also show that the adsorption behavior is dominated by chemisorption, which is consistent with the results of the pseudo-second-order kinetic model[45,50]. In addition, in Elovich model, the value of a (26.722) is greater than that of b (0.14), indicating that TC molecules can stably bind to the adsorption site of MBC, and MBC has strong stability in the adsorption of TC[51]. The intra-particle model (Fig. 12a) reveals that the adsorption process occurs in three stages: Stage I is liquid film diffusion; Stage II is intra-particle diffusion. Stage III achieves equilibrium. The adsorption rate of Stage I is controlled by the diffusion of molecules in the TC solution. Stage II is mainly controlled by chemisorption. In addition, the fitting line of intra-particle diffusion does not pass through the coordinate origin, which indicates that intra-particle diffusion is not the only control step for the adsorption rate of TC by MBC, and other mechanisms may also be involved[45].

The mathematical expressions of Quasi-first-order (1), Quasi-second-order (2), Elovich (3) and Intra-particle diffusion model (4) are as follows:

$$Q_t = Q_e\left(1 - \exp^{-k_1 t}\right) \tag{1}$$

$$Q_t = \frac{Q_e^2 k_2 t}{1 + Q_e k_2 t} \tag{2}$$

$$Q_t = \frac{1}{b}\ln(ab) + \frac{1}{b}\ln t \tag{3}$$

$$Q_t = k_3 t^{0.5} + C \tag{4}$$

t—contact time, min;

Q_t—adsorption capacity of MBC at t time, mg g^{-1};

Q_e—adsorption capacity at the moment when adsorption reaches equilibrium, mg g^{-1};

k_1—the adsorption rate constant, min^{-1};

k_2—the adsorption rate constant, g mg^{-1} min^{-1};

k_3—the adsorption rate constant, mg g^{-1} $min^{0.5}$;

a, b—the adsorption rate constants.

The isothermal adsorption experiment was carried out in the range of TC initial concentration 10–100 mg/L, with the following experimental conditions: MBC dosage 30 mg, pH = 7, adsorption temperature 20 °C. The Freundlich and Langmuir models were used to fit the experimental data, and the results are shown in Fig. 12b, with the corresponding parameters presented in Table 3. For fitted models, the square of correlation coefficient (R^2) was used to evaluate the fitting results. It can be seen from Table 3 that the obtained R^2 values are all ≥ 0.931, indicating that both models can describe the adsorption of TC by MBC well. These results suggest that the adsorption of TC on MBC involves two processes: monolayer adsorption (Langmuir model) and multilayer adsorption (Freundlich model). K_L of Langmuir model can represent the favorable degree of adsorption, which can be divided into four cases: when $K_L > 1$, adsorption is unfavorable; When $K_L = 1$, linear adsorption; When $0 < K_L < 1$, the adsorption is favorable. When $K_L = 0$, irreversible adsorption[52]. Since the obtained K_L is less than 1, it indicates that the adsorption reaction of TC is favorable on MBC. For the Freundlich model, the parameter n also represents the favorable degree of adsorption. When n is greater than 1.0, the adsorption is favorable at high concentration and unfavorable at low concentration. When n is less than 1.0, adsorption is favorable throughout the concentration range[53]. As shown in Table 3, the n value is 4.31, indicating that the adsorption of TC by MBC is favorable in the high-concentration range.

Freundlich model (5) and Langmuir model (6) are expressed in the following mathematical formula:

$$Q_e = K_F C_e^{1/n} \tag{5}$$

$$Q_e = \frac{Q_m K_L C_e}{1 + (K_L C_e)} \tag{6}$$

C_e—solution concentration after equilibrium of adsorption reaction, mg/L;
Q_e—adsorption capacity of magnetic biomass to TC during adsorption equilibrium, mg g^{-1};
Q_m—the theoretical maximum adsorption capacity, mg g^{-1};
k_F k_L and n are all constants;

The adsorption mechanism of MBC on TC was analyzed by thermodynamic method, and the influence of temperature on the adsorption performance was further explored. The parameters of ΔG, ΔH, ΔS derived from Gibbs–Helmholtz are presented in Table 4. The negative value of ΔG implies that TC adsorption by MBC occurrs spontaneously. Furthermore, the decreasing ΔG with increasing temperature, combined with the positive ΔH value, confirm that higher temperatures favor the adsorption of TC onto MBC. According to the study of Yao et al.[54], the adsorption process of $-20 < \Delta G < 0$ kJ/mol and $0 < \Delta H < 40$ kJ/mol is closely related to the physical interaction. $\Delta S > 0$ suggests an increase in randomness and affinity at the solid–liquid interface, which reveals certain changes in MBC surface and TC molecular structure[55].

SEM characterization (Fig. 1) results showed that MBC had a well-developed pore structure, which was conducive to TC diffusion from the surface of the adsorbent to the interior by pore filling. Zeta potential test and adsorption experiments at different pH indicate that electrostatic action plays an indispensable role in the adsorption between MBC and TC. For details, see the "Analysis of influencing factors on TC removal" section above. The comparison of FT-IR spectra before and after adsorption of TC (Fig. 4) is helpful in analyzing the changes of surface functional groups and provide support for the analysis of adsorption mechanism. After adsorption of TC, the peak intensity at 773–780 cm^{-1} is significantly enhanced, which is attributed to the C–H bending vibration of the benzene ring in TC[56]. The shifts of the peaks of OH and C–O at 3430 ~ 3440 and 993–996 cm^{-1} and the intensity changes indicate that TC is successfully absorbed on MBC[38]. At the same time, the tensile vibration of C = C (1330–1350 cm^{-1}) increases significantly, which is mainly due to the π-π interaction between the conjugated benzene ring of TC and the aromatic ring of MBC during adsorption[57]. The variation of Fe–O peak intensity may be due to the surface complexation of MBC with TC and the participation of Fe–O in the reaction[58]. It can be inferred from the above analysis that the adsorption between MBC and TC involves the interaction of surface complexation and π-π interaction.

The XPS analysis of MBC (Fig. 5) after TC adsorption was used to further elaborate the possible mechanism. After adsorption of TC, the binding energy positions of C 1 s, O1s and Fe 2p shift to the right, which is due to the chemical shift caused by charge transfer and electrostatic interaction between MBC and TC[58]. In C-1 s, it was found that the binding energy positions and the area ratios of oxygen-containing functional groups changed after TC adsorption. Specifically, the area ratios of C–O and O–C = O increased from 23.68 and 3.95% to 32.59 and 8.15%, respectively, while the ratios of C = C, C = O, and π-π bonds decreased from 50.18, 13.91, and 8.28 to 45.68, 7.76, and 5.82%[59]. The results show that these oxygen-containing functional groups may play a key role in the adsorption process of TC by MBC, and the adsorption may involve π-π interactions, hydrogen bonding, and hydrophobic effects[42,43]. In addition, the area ratio of Fe–O bond in O-1 s decreased from 20.06% to 15.53%, indicating that this group is the main adsorption site for MBC. The analysis of Fe 2p showed that the valence composition of the element changes obviously, which may be due to the interaction of the strong oxidized hydroxyl groups in TC with the iron oxide nanoparticles[60]. Based on the above analysis, the possible adsorption mechanisms of MBC include pore filling, electrostatic attraction, π-π interaction, hydrogen-bonding, and surface complexation of the surface functional groups.

Removal performance of different pollutants

In this study, MG was selected as the representative material of organic dyes, and Pb^{2+} was selected as the representative material of heavy metal pollutants, to carry out adsorption performance research, and explore the effectiveness of MBC material for the removal of different types of pollutants. As can be seen in Fig. 13, the adsorption capacity of MBC material prepared in this study is up to 194.8 mg/g, which is slightly higher than the materials prepared by our research group using $FeCl_3$ and $FeSO_4$ as precursors and chemical co-precipitation method[61]. The adsorption capacity of Pb^{2+} is 97.3 mg/g, which is similar to the results obtained by Sun[62] using $FeCl_3$ and rice husk as raw materials and one-step pyrolysis method. It can be seen that the MBC material prepared in this study has good adsorption performance for tetracycline, organic dyes and heavy metals. While the actual water quality and pollutant types may vary, and this material has the potential for application in actual water bodies.

T(K)	△G/(KJ/mol)	△H/(KJ/mol)	△S/[J(mol·K)$^{-1}$]
293	−6.351	38.347	152.188
298	−6.781		
303	−7.883		

Table 4. Thermodynamic parameters for TC adsorption on MBC (TC 30 mg/L, pH = 7, MBC 30 mg).

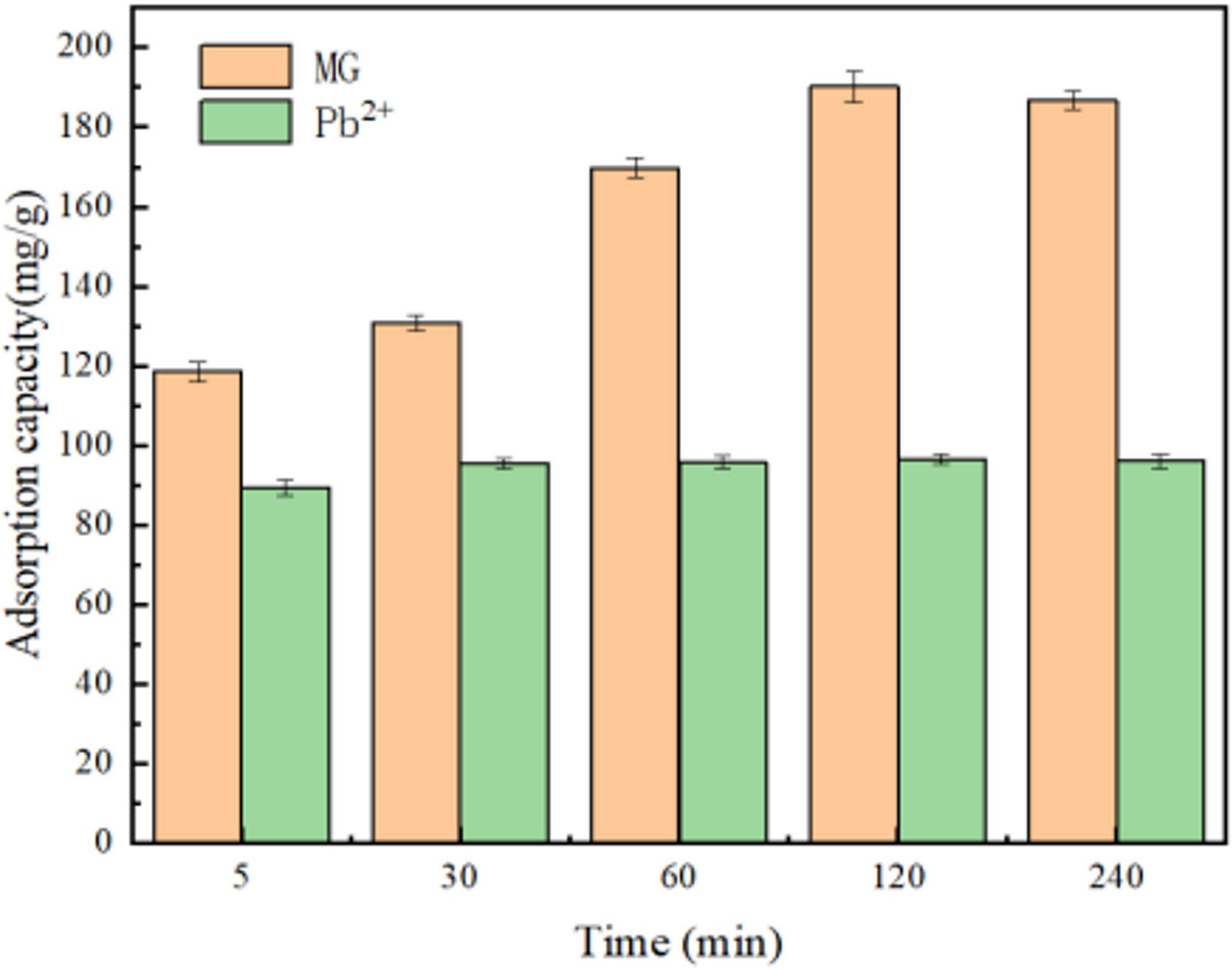

Fig. 13. Removal performance of MBC on different pollutants (MBC 10 mg, pH = 7.0, T = 20 °C, MG 50 mg/L/ Pb^{2+} 20 mg/L).

Pollutant	Sample 1	Sample 2	Sample 3
pH	7.8	7.8	7.7
COD_{Mn} (mg/L)	4.4	4.4	4.9
NH_3–N (mg/L)	0.519	0.538	0.535
SO_4^{2-} (mg/L)	83.0	83.6	82.0
Cl^- (mg/L)	24.8	24.4	23.9
CO_3^{2-} (mg/L)	2.15	1.78	2.97
HCO_3^- (mg/L)	19.2	20.1	17.1

Table 5. Real water quality.

Applications in real water

In order to explore the potential application of MBC in real water bodies, we collected water samples from the lower reaches of the Yiluo River for adsorption experiments. The Yiluo River is one of the ten major tributaries of the Yellow River. The river basin has experienced intense human activities over a long history. In the context of climate change and increasing water intake, the development of metal minerals in the upper reaches, as well as agricultural and urban non-point source discharge in the middle and lower reaches, have posed long-term threats to the water environment[63,64]. Lead is a kind of heavy metal with strong toxicity released by lead–zinc, molybdenum and gold mining industries in the upper reaches of Yiluo River[65]. The study of related environmental risks have shown that the content of lead in streams from the mining area have reached the warning level[66]. Table 5 shows the chemical measurement results of the actual water body, pH 7.7–7.8, COD_{Mn} 4.4–4.9 mg/L, NH_3–N

0.519–0.535 mg/L, all of which meet the requirements of the "Surface Water Environmental Quality Standard" (GB3838-2002) Class III. Since the sampling point is located in downstream of the Yiluo River and receives a large amount of tail water from sewage treatment plants along the line, the actual water body contains a variety of inorganic ions and dissolved organic matter, which can interfere with the removal of target pollutants—a common challenge faced by water treatment technologies. As shown in Fig. 14, the representative pollutants in the actual water body (TC spiked 10 mg /L, MG spiked 50 mg /L, Pb^{2+} spiked 20 mg/L) were effectively removed, with removal rates exceeding 80%, especially for Pb^{2+}, which had a removal rate above 95%. These results demonstrate the wide application potential of the adsorbent material developed in this study.

Generality of preparation method

Using peanut shell and red mud as raw materials, MBC can be prepared in one step by the dry mixing pyrolysis method, which shows good adsorption properties, solid–liquid separation performance, and reusability. In order to explore whether this simple preparation method is effective for a wide variety of biomass, this study selected straw of important oil crops—soybean and cash crops—pepper as raw materials, combined with red mud in different proportions, and subjected to the dry pyrolysis to produce MBC (named SS/RM-BC and PS/RM-BC, respectively). The two types of MBC were pyrolyzed at 700 °C for 2 h under oxygen limited conditions, which is exactly the same as the preparation method of peanut shell MBC. The adsorption properties of various MBC are shown in Fig. 15.

As can be seen from the figure, the adsorption performance of PS/RM-BC is generally stronger than that of SS/RM-BC under 700 °C and oxygen limited conditions. Among all PS/RM-BC materials, the adsorption performance of pepper straw and red mud prepared in 1:1 ratio is the best, with a maximum adsorption capacity is 40.1 mg/g. Among all SS/RM-BC materials, the 2:1 ratio of soybean straw and red mud has the best adsorption performance, and the maximum adsorption capacity is 35.5 mg/g. Interestingly, among the two types of composite materials, the combination with the weakest adsorption capacity is the combination with the highest content of RM. Loebsack et al.[23] used MBC prepared by pyrolysis of Canadian pine and red mud in different proportions to adsorb acetaminophen. The results showed that as the content of RM increased, its adsorption capacity gradually decreased, and red mud mainly played a role as a magnetic precursor in the material preparation process.

The adsorption properties of these materials have been improved compared to the materials prepared by chemical co-precipitation method using peanut shell, $FeCl_3$ and $FeSO_4$ (Q_{max} 33.5 mg/g) before by our research group[12]. The adsorption capacity of these two kinds of materials is similar to that of the magnetic biochar

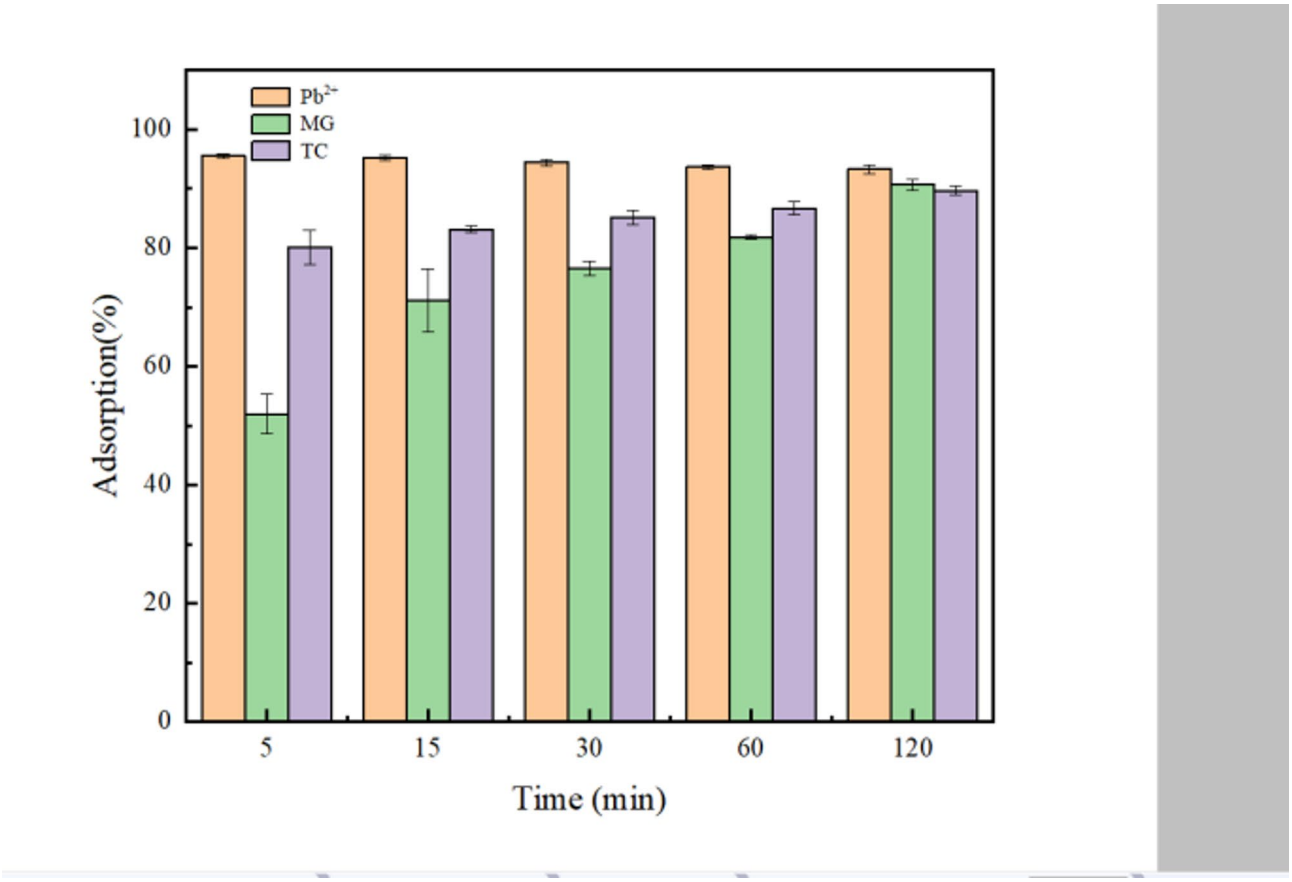

Fig. 14. Pollutant removal performance in real water (MBC 10 mg, T = 20 °C).

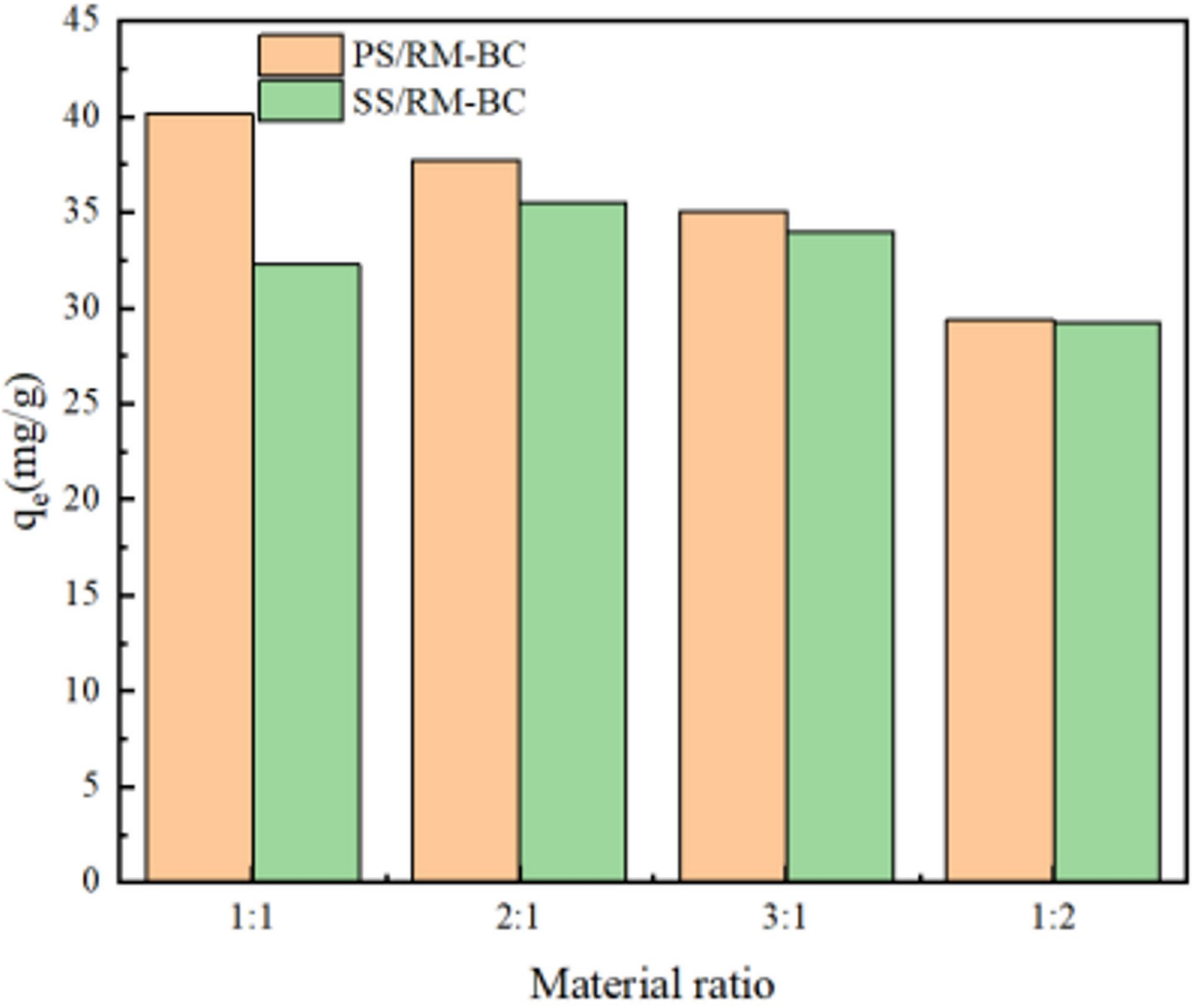

Fig. 15. Adsorption performance of different biomass materials (Dosage of adsorbent 30 mg, pH = 7.0, TC 30 mg/L, T = 20 °C).

materials (37.95 mg/g) prepared by Wang[67] using Spent mushroom substrate of Lentinus edodes and hexavalent ferric salt by a two-step impregnation-pyrolysis method. It can be seen that the one-step pyrolysis method exhibited good generality for the preparation of MBC from different biomass.

Comparison of adsorption performance with relevant studies

We reviewed the recently published literature on magnetic activated carbon adsorption of TC, focusing on raw materials, preparation methods and performance parameters, the results are summarized in Table 6.

As can be seen from Table 6, in order to obtain magnetic activated carbon materials with excellent adsorption capacity, the biomass is often treated with strong oxidizing agents, such as ferrate, or nitrogen-rich chemicals like urea and melamine, during the carbonization process. This helps generate a rich surface of functional groups. Additionally, the incorporation of pore-forming agents (e.g., CH_3COOK, $ZnCl_2$, KOH, $NaHCO_3$) during pyrolysis enables the biomass to develop a well-structured porous network. It is worth noting that the preparation process of these adsorbent materials often involves high chemical inputs, wastewater discharge, and complex operational steps. The adsorption capacity of the MBC prepared in this study is at a medium level, but the environment friendliness is outstanding, as no chemicals are added, and no waste water is generated. By comparing the specific surface area of the materials, we found that the pore structure of MBC could be further improved. In the future, we plan to increase the adsorption capacity of the materials by adding industrial wastes with pore making functions.

Preparation cost estimation

The recent literature on the preparation cost of magnetic biochar adsorbed TC was reviewed and analyzed, with the adsorption capacity and preparation cost summarized in Table 7. However, these previous studies largely

Materials	Preparation method	Adsorption capacity of TC (mg/g)	Specific surface area (m^2/g)	References
Kelp:K_2FeO_4 = 1:1.5	Hydrothermal carbonization, details are as follows: Kelp powder, purchased potassium ferrate and ultra-pure water were stirred evenly in a flange reactor and heated in a Muffle furnace at 300 °C	1245.43	353.5	10
Corncob, CH_3COOK, $FeCl_3{\cdot}6H_2O$, and $C_3H_6N_6$	One-step pyrolysis, details are as follows: After dry mixing, the four raw materials were pyrolyzed with N_2 in a tube furnace at 800 °C for 1 h	764.35	2083.54	15
Municipal sludge, $CO(NH_2)_2$, $FeCl_3{\cdot}6H_2O$	Pyrolysis + hydrothermal activation, details are as follows: Biochar was prepared by N_2 protection pyrolysis of municipal sludge in a tube furnace, and then activated at 220 °C for 12 h with $CO(NH_2)_2$ and $FeCl_3$ solution	197.3	243	40
Sugarcane bagasse, Red mud, $C_3H_6N_6$, $NaHCO_3$	Four kinds of raw materials dry mixing grinding; One step pyrolysis with N_2 at 700 °C	143.9	279.1	45
Rice waste, $ZnCl_2$ and $FeCl_3$	Hydrothermal + pyrolysis, the specific steps are as follows: rice flour and deionized water are heated at 230 °C in a hydrothermal autoclast for 3 h, the filtered product is impregnated with $ZnCl_2$ and $FeCl_3$ in solution for 16 h, and finally pyrolyzed in a tube furnace under nitrogen protection for 90 min	94.63	747.76	38
Red mud, Peanut shell	One-step pyrolysis, details are as follows: red mud and peanut shells were mixed evenly after grinding, and pyrolyzed at 700 °C in Muffle furnace for 2h under oxygen limited conditions	87.39	113.75	Present study
Nano-zero-valent iron, sewage sludge	Pyrolysis, details are as follows: dry sludge and zero-valent iron are heated in a Muffle furnace under N_2 protection at 500 °C for 2.5 h	81.04	–	16
Peanut shell, $FeCl_3$ and $FeSO_4$	Pyrolysis + co-precipitation, details are as follows: Peanut shells were pyrolyzed at 500 °C in Muffle furnace for 2 h under oxygen limited conditions, and biochar powder, $FeCl_3$ and $FeSO_4$ were stirred in water at 55 °C for 30 min	71.43	122.1	12
Poplar fine powder, $NH_4Fe(SO_4)_2$, KOH	Pyrolysis + co-precipitation, details are as follows: The pulverized poplar fine powder was activated in KOH solution, and then pyrolyzed in vacuum tube furnace at 1500 °C for 2 h. The obtained biochar was stirred in $NH_4Fe(SO_4)_2$ solution at 50 °C for 12 h	70.28	122.12	11
Spent mushroom substrate of Lentinus edodes , K_2FeO_4	Pyrolysis + co-precipitation + Pyrolysis, details are as follows: Spent mushroom substrate of Lentinus edodes was heated at 500 °C in Muffle furnace for 3 h under oxygen restriction.The biochar was immersed in K_2FeO_4 solution at room temperature and stirred for 12 h, and then pyrolyzed in Muffle furnace at 500 °C for 3 h	37.95	373.29	67
Red mud, Peanut shell, HNO_3	One-step pyrolysis, details are as follows:Red mud powder, peanut shell powder and nitric acid were stirred in water for 30 min, and the filtered solids were pyrolyzed at 700 °C under N_2 protection in a tube furnace for 2 h	12	36.77	68

Table 6. Comparison of adsorption performance with relevant studies.

Price (USD/kg)	Adsorption capacity of TC (mg/g)	Materials and preparation method		References
5.677	87.39	Red mud, peanut shell; dry mixed pyrolysis	Energy consumption(including pyrolysis, drying, grinding) 3.84 USD/kg	Present study
			Transportation 0.8 USD/kg	
			Labour cost 0.357USD/kg	
			Capital investment cost 0.68 USD/kg	
5.91	94.63	Rice waste as raw material, commercial $ZnCl_2$ and $FeCl_3$ as magnetic precursors; hydrothermal carbonization		38
5.2	71.43	Peanut shell, $FeCl_3$ and $FeSO_4$; chemical coprecipitation		12
52.59	143.9	Sugarcane bagasse, Red mud, $C_3H_6N_6$, $NaHCO_3$; One step pyrolysis		45

Table 7. Preparation cost.

overlooked the labor cost and capital investment, as they were conducted at the laboratory scale, with batch outputs typically in the range of a few grams. Before commercial-scale production, the preparation process needs to be scaled up. The production cost of commercial activated carbon includes equipment fixed assets, labor, raw materials, and operating costs[69]. At the laboratory stage, it is challenging to perform a complete economic analysis of biochar production. For the MBC prepared in this study, we estimated the labor cost at $0.357 / kg and capital investment cost at $0.68 / kg. Personnel operating time is around 10 min, mainly the switching of the Muffle furnace and the filling of materials, and the labor cost is 0.357 USD/kg according to the hourly wage of ordinary workers. The Muffle furnace, with a design life of 99,000 h and a cost of $1,715, amounts to $0.017/h. Each batch takes 2h to produce approximately 50 g of MBC, leading to an estimated capital investment cost of $0.68/kg. In summary, the total cost of material preparation in this study is $5.677 / kg. Even compared with the materials reported above, which do not consider the cost of labor and capital investment cost, the cost of material preparation in this study is still lower. However, it should be noted that energy consumption accounts for over 67% of the total cost. With the expansion of the preparation scale and optimization of energy consumption, the preparation cost is expected to be gradually reduced[70]. In the next step, we plan to carry out material preparation experiments at the kilogram scale to continuously improve the application potential of MBC.

Conclusion

Using RM as magnetic precursor and peanut shell as substrate, magnetic biochar (MBC) for TC removal from water was successfully prepared via a one-step pyrolysis method. The MBC showed adaptability to the

adsorption of antibiotics in a wide pH range (3–11), and the presence of organic ion HA had a more significant effect on the adsorption capacity than inorganic ion. Chemisorption was identified as the dominant adsorption mechanism, which is an endothermic and spontaneous process. The material demonstrated good solid–liquid separation performance, with the TC removal rate remaining above 70% after 4 consecutive uses. Importantly, all raw materials were made from solid waste, significantly reducing the preparation costs. The material also exhibited a good removal effect on heavy metals and dyes in actual water, demonstrating its application potential. Furthermore, the magnetic biochar prepared with pepper straw and soybean straw as raw materials showed good adsorption effect which indicates the universal applicability of the one-step pyrolysis preparation method across different waste biomass sources.

Materials and methods

Preparation of materials

One-step pyrolysis method was used to prepare MBC. Peanut shells from a farm in Kaifeng City, Henan Province, China were cleaned, dried, crushed, screened with 80 mesh screens for reserve use. RM collected from an aluminum oxide plant in Sanmenxia City, Henan Province, China was dried, crushed and screened with a 100-mesh screen for reserve use. The treated RM and peanut shells were mixed evenly at a mass ratio of 1:2 and then put into a crucible and placed in a box Muffle furnace. MBC was obtained by pyrolysis at 5 °C/min at 700 °C for 2 h under oxygen limited conditions.

Sample characterization

The morphology of the prepared MBC material was observed using a field emission scanning electron microscope (SEM) produced by Zeiss, Germany, with a magnification of 40,000 times. The crystal structure was analyzed by X-ray diffraction (XRD) mode (D8 Bruker, GER). The Cu Kα1 ray is used, with a wavelength of 0.154 nm for diffraction. Chemical structure in the 400–4000 cm^{-1} regions was determined in vacuum by Fourier transform infrared (FT-IR) spectroscopy (IS5) from Thermo fisher, USA. High-resolution X-ray photoelectron spectrometer (XPS; AXIS Ultra DLD, UK) was used to analyze the chemical composition of samples of MBC as well as the changes in chemical valence and surface element content. The charge was corrected by using the energy standard C 1 s = 284.80 eV. The specific surface area, pore size distribution and specific pore volume of MBC were analyzed by Micromeritics ASAP2460 specific surface area analyzer.

Adsorption experiment

In order to explore the treatment effect of TC in actual water, the effects of MBC dosage, initial concentration of TC solution, pH, temperature and typical coexisting ions on the adsorption performance were investigated. In order to ensure the accuracy of the experiment, parallel experiments were carried out for the adsorption experiments with the influence of environmental factors on the adsorption properties, and each group was repeated three times. All adsorption experiments were carried out in a 250 ml conical bottle filled with 50 ml of solution, and the conical bottle was subjected to a magnetic stirrer at 150 rpm. After the adsorption, the mixture was separated by a magnet and the liquid was filtered by a 0.45 μm membrane. The conditions and methods of each experiment are as follows:

(1) Analysis of influencing factors on TC removal.

① Effect of MBC dosage on adsorption: initial concentration of TC solution 30 mg/L, T = 20 °C and pH = 7; ② Effect of initial concentration of TC solution: MBC dosage 30 mg, T = 20 °C and pH = 7; ③ Effect of pH: initial concentration of TC solution 30 mg/L, MBC dosage 30 mg and T = 20 °C; The pH of the solution was adjusted using 0.2 mol/L HCl and 2 mol/LNaOH solutions. ④ Effect of water temperature: initial concentration of TC solution 30 mg/L, MBC dosage 30 mg and pH = 7; ⑤ Effect of coexisting ions: At MBC dosage of 30 mg, TC concentration of 30 mg/L and water temperature of 20 °C, $NaNO_3$, Na_2SO_4, NaCl, $NaHCO_3$ and Na_2CO_3 were added respectively to form corresponding ion concentration solutions to carry out adsorption experiments.

(2) Removal mechanism of TC in water.

① Adsorption kinetics experiment: The adsorption experiment was carried out under the conditions of 30 mg MBC dosage, 30 mg/L initial TC concentration, pH = 7 and water temperature T = 20 °C. The absorbance of the solution was measured at 2, 5, 10, 15, 30, 45, 60, 90 and 120 min. ② Adsorption isothermal experiment: under the conditions of solution temperature T = 20 °C, pH = 7, and MBC dosage of 30 mg, the adsorption experiments were carried out at the solution concentration of 10, 20, 30, 50, 65, 80, and 100 mg/LTC, respectively, and the absorbance of the solution was measured after 2 h adsorption. ③ Adsorption thermodynamic experiment: Under the conditions of initial TC concentration of 30 mg/L, pH = 7 and MBC dosage of 30 mg, the adsorption experiments were carried out at solution temperature of 20, 25 and 30 °C respectively, and the absorbance of the solution was measured after 2 h of adsorption.

(3) Removal experiments of different pollutants: MBC 10 mg, pH = 7.0, T = 20 °C, MG 50 mg/L, Pb^{2+} 20 mg/L;
(4) Real water removal experiment: After adding three types of representative pollutants (TC spiked 10 mg /L, MG spiked 50 mg /L, Pb^{2+} spiked 20 mg/L) to water samples collected from Yiluo River, MBC 10 mg was added, and the concentration of pollutants in the solution was determined after 2 h adsorption.

(5) The pollutant adsorption experiment of different biomass materials: under the conditions of TC 30 mg/L, pH = 7.0, T = 20 °C, different biochar materials were added respectively, and the pollutant concentration in the solution was determined after adsorption for 2 h.

The absorbance of TC and MG in the filtrate were determined by T9CS UV–VIS spectrophotometer of Beijing Puxi General Instrument Co., LTD. The absorption wavelengths of TC and MG were 355 nm and 617 nm respectively. The concentration of lead ion in the filtrate was determined by AA-7000 atomic absorption spectrophotometer produced in Shimadzu, Japan, and its characteristic spectral line was 283.3 nm.

Analysis of the removal mechanism of TC by MBC

After MBC adsorbed TC in water, the isotherm model, adsorption kinetic model and thermodynamics were respectively used to analyze the adsorption process of TC by MBC. The equations of the model used for adsorption kinetics and isotherm fitting have been given above, and are detailed in Eqs. (1)–(6).

Data availability

All data generated or analyzed during this study are included in this published article and supporting information.

Received: 9 July 2024; Accepted: 31 July 2025
Published online: 17 August 2025

References

1. Zhang, X. et al. Contamination distribution and non-biological removal pathways of typical tetracycline antibiotics in the environment: A review. *J. Hazard. Mater.* **463**, 132862. https://doi.org/10.1016/j.jhazmat132862 (2023).
2. Antos, J., Piosik, M., Ginter-Kramarczyk, D., Zembrzuska, J. & Kruszelnicka, I. Tetracyclines contamination in European aquatic environments: A comprehensive review of occurrence, fate, and removal techniques. *Chemosphere* **353**, 141519. https://doi.org/10.1016/j.chemosphere141519 (2024).
3. Martin, V., Bettencourt, A. F., Santos, C. & Gomes, P. S. Reviewing particulate delivery systems loaded with repurposed tetracyclines–from micro to nanoparticles. *Int. J. Pharm.* **649**, 123642. https://doi.org/10.1016/j.ijpharm123642 (2023).
4. Liao, Q. et al. Interaction between tetracycline and microorganisms during wastewater treatment: A review. *Sci. Total Environ.* **757**, 143981. https://doi.org/10.1016/j.scitotenv143981 (2020).
5. Kong, D. et al. Cathodic degradation of antibiotics: Characterization and pathway analysis. *Water Res.* **72**, 281–292. https://doi.org/10.1016/j.watres.2015.01.025 (2015).
6. Carvalho, I. T. & Santos, L. Antibiotics in the aquatic environments: A review of the European scenario. *Environ. Int.* **94**, 736–757. https://doi.org/10.1016/j.envint.2016.06.025 (2016).
7. Gothwal, R. & Shashidhar, T. Antibiotic pollution in the environment: A review. *Clean-Soil Air Water* **43**(4), 479–489. https://doi.org/10.1002/clen.201300989 (2015).
8. Suyamud, B. et al. Antimicrobial resistance in aquaculture: Occurrence and strategies in Southeast Asia. *Sci. Total Environ.* **907**, 167942. https://doi.org/10.1016/j.scitotenv167942 (2024).
9. Minale, M. et al. Application of graphene-based materials for removal of tetracyclines using adsorption and photocatalytic-degradation: A review. *J. Environ. Manag.* **276**, 111310. https://doi.org/10.1016/j.jenvman111310 (2020).
10. Hang, J. et al. A super magnetic porous biochar manufactured by potassium ferrate-accelerated hydrothermal carbonization for removal of tetracycline. *J. Clean. Prod.* **435**, 140470. https://doi.org/10.1016/j.jclepro140470 (2023).
11. Zhang, X. et al. An achieved strategy for magnetic biochar for removal of tetracyclines and fluoroquinolones: Adsorption and mechanism studies. *Bioresour. Technol.* **369**, 128440. https://doi.org/10.1016/j.biortech128440 (2022).
12. Zhang, Q. et al. Effect on the adsorption performance and mechanism of antibiotics tetracyclines by the magnetic biochar used peanut shells as raw materials. *Mater. Res. Express* **11**, 045508. https://doi.org/10.1088/2053-1591/ad3719 (2024).
13. Xu, X., Zheng, Y., Gao, B. & Cao, X. N-doped biochar synthesized by a facile ball-milling method for enhanced sorption of CO_2 and reactive red. *Chem. Eng. J.* **368**, 165. https://doi.org/10.1016/j.cej02.165 (2019).
14. Tang, J. et al. Fe–Al bimetallic oxides functionalized-biochar via ball milling for enhanced adsorption of tetracycline in water. *Bioresour. Technol.* **369**, 128385. https://doi.org/10.1016/j.biortech128385 (2022).
15. Deng, Y. et al. One-step synthesis of iron and nitrogen co-doped porous biochar for efficient removal of tetracycline from water: Adsorption performance and fixed-bed column. *J. Environ. Manag.* **352**, 119984. https://doi.org/10.1016/j.jenvman.2023.119984 (2024).
16. Hu, T. et al. Potential removals of tetracycline and sulfamethoxazole by iron-loaded sludge biochar. *J. Water Process.* **54**, 103962. https://doi.org/10.1016/j.jwpe.2023.103962 (2023).
17. Zhong, H. et al. When biochar meets iron mineral: An opportunity to achieve enhanced performance in treating toxic metal(loid)s and refractory organics. *Sep. Purif. Technol.* **350**, 128022. https://doi.org/10.1016/j.seppur128022 (2024).
18. Zhou, L. et al. Endogenous iron-enriched biochar derived from steel mill wastewater sludge for tetracycline removal: Heavy metals stabilization, adsorption performance and mechanism. *Chemosphere* **359**, 142263. https://doi.org/10.1016/j.chemosphere142263 (2024).
19. Cusack, P. B., Courtney, R., Healy, M. G., Donoghue, L. M. T. O. & Ujaczki, É. An evaluation of the general composition and critical raw material content of bauxite residue in a storage area over a twelve-year period. *J. Clean. Prod.* **208**, 083. https://doi.org/10.1016/j.jclepro10.083 (2018).
20. Zhou, Y. et al. Roles of red mud in remediation of contaminated soil in mining areas: Mechanisms, advances and perspectives. *J. Environ. Manag.* **356**, 120608. https://doi.org/10.1016/j.jenvman120608 (2024).
21. Wang, J., Liu, X., Zhang, Z. & Liu, Y. Synergistic utilization, critical mechanisms, and environmental suitability of bauxite residue (red mud) based multi-solid wastes cementitious materials and special concrete. *J. Environ. Manag.* **361**, 121255. https://doi.org/10.1016/j.jenvman121255 (2024).
22. Xue, S. et al. Effect of phosphogypsum and poultry manure on aggregate-associated alkaline characteristics in bauxite residue. *J. Environ. Manag.* **256**, 109981. https://doi.org/10.1016/j.jenvman109981 (2019).
23. Loebsack, G. et al. Adsorption mechanisms and optimal production of magnetic biochar composites from red mud and soft wood biomass. *J. Anal. Appl. Pyrolysis.* **177**, 106340. https://doi.org/10.1016/j.jaap106340 (2023).
24. Ahmed, W. et al. Adsorption of Pb(II) from wastewater using a red mud modified rice-straw biochar: Influencing factors and reusability. *Environ. Pollut.* **326**, 121405. https://doi.org/10.1016/j.envpol121405 (2023).
25. Yang, J. et al. Functional biochar fabricated from red mud and walnut shell for phosphorus wastewater treatment: Role of minerals. *Environ. Res.* **232**, 116348. https://doi.org/10.1016/j.envres116348 (2023).

26. Feng, X. et al. Spatio-temporal dynamics of global peanut production and trade. *Hua Sheng Xue Bao* **50**, 1–8. https://doi.org/10.14001/j.issn.1002-4093.2021.04.001 (2021).
27. Kumar, M. et al. Pyrolysis of peanut shell: Kinetic analysis and optimization of thermal degradation process. *Ind. Crops. Prod.* **174**, 114128. https://doi.org/10.1016/j.indcrop114128 (2021).
28. Bharath, G. et al. Enhanced electrochemical performances of peanut shell derived activated carbon and its Fe_3O_4 nanocomposites for capacitive deionization of Cr(VI). *Sci. Total Environ.* **691**, 069. https://doi.org/10.1016/j.scitotenv07.069 (2019).
29. Renita, A. A., Amarnath, D. J. & Duraikannu, S. L. Synthesis of peanut-shell magnetized biocarbon for acid fuchsin dye removal. *Mater. Today Proc.* **43**, 407. https://doi.org/10.1016/j.matpr.2021.01.407 (2021).
30. Kumar, A., Upadhyay, S. N., Mishra, P. K. & Mondal, M. K. Multivariable modeling, optimization and experimental study of Cr(VI) removal from aqueous solution using peanut shell biochar. *Environ. Res.* **215**, 114287. https://doi.org/10.1016/j.envres114287 (2022).
31. Xu, B. et al. Acid-modified red mud biochar for the degradation of tetracycline: Synergistic effect of adsorption and nonradical activation. *J. Environ. Manag.* **347**, 119077. https://doi.org/10.1016/j.jenvman.2023.119077 (2023).
32. Deng, S. et al. Treatment of dyes wastewater by the catalytic wet persulfate oxidation process in reactors using red mud combined with biochar as catalyst. *Water Air Soil Pollut.* **234**(9), 573. https://doi.org/10.1007/s11270-023-06555-7 (2023).
33. Rajahmundry, G. K. et al. Statistical analysis of adsorption isotherm models and its appropriate selection. *Chemosphere* **276**, 130176. https://doi.org/10.1016/j.chemosphere130176 (2021).
34. Dang, A. et al. High-efficient adsorption for versatile adsorbates by elastic reduced graphene oxide/Fe_3O_4 magnetic aerogels mediated by carbon nanotubes. *J. Hazard. Mater.* **457**, 131846. https://doi.org/10.1016/j.jhazmat131846 (2023).
35. Yan, B., Niu, H. C. & Wang, J. Kinetics, electron-donor-acceptor interactions, and site energy distribution analyses of norfloxacin adsorption on pretreated barley straw. *Chem. Eng. J.* **330**, 056. https://doi.org/10.1016/j.cej08.056 (2017).
36. Yoon, K. et al. Synthesis of functionalised biochar using red mud, lignin, and carbon dioxide as raw materials. *Chem. Eng. J.* **361**, 1597–1604. https://doi.org/10.1016/j.cej.2018.11.012 (2019).
37. Monfort, F. et al. Development of anodic coatings on aluminium under sparking conditions in silicate electrolyte. *Corros. Sci.* **49**, 672–693. https://doi.org/10.1016/j.corsci.2006.05.046 (2007).
38. Zhang, F. et al. Effective removal of tetracycline antibiotics from water by magnetic functionalized biochar derived from rice waste. *Environ. Pollut.* **330**, 121681. https://doi.org/10.1016/j.envpol121681 (2023).
39. Li, X. et al. Rapid and efficient adsorption of tetracycline from aqueous solution in a wide pH range by using iron and aminoacetic acid sequentially modified hierarchical porous biochar. *Bioresour. Technol.* **346**, 126672. https://doi.org/10.1016/j.biortech126672 (2022).
40. Ma, Y. et al. One-pot hydrothermal synthesis of magnetic N-doped sludge biochar for efficient removal of tetracycline from various environmental waters. *Sep. Purif. Technol.* **297**, 121426. https://doi.org/10.1016/j.seppur121426 (2022).
41. Xu, Z. et al. Simultaneous removal of phosphate and tetracycline using $LaFeO_3$ functionalised magnetic biochar by obtained ultrasound-assisted sol–gel pyrolysis: Mechanisms and characterisation. *Environ. Res.* **239**, 117227. https://doi.org/10.1016/j.envres117227 (2023).
42. Asiyeh, K. et al. Design and preparation magnetic bio-surfactant rhamnolipid-layered double hydroxide nanocomposite as an efficient and recyclable adsorbent for the removal of Rifampin from aqueous solution. *Sep. Purif. Technol.* **304**, 122362. https://doi.org/10.1016/j.seppur122362 (2022).
43. Zhao, N. et al. Chlortetracycline hydrochloride removal by different biochar/Fe composites: A comparative study. *J. Hazard. Mater.* **403**, 123889. https://doi.org/10.1016/j.jhazmat123889 (2020).
44. Zhang, Q. et al. Photocatalytic degradation of tetracycline antibiotics using three-dimensional network structure perylene diimide supramolecular organic photocatalyst under visible-light irradiation. *Appl. Catal. B.* **277**, 119122. https://doi.org/10.1016/j.apcatb119122 (2020).
45. Zhang, L. et al. Novel magnetic N-doped biochar derived from sugarcane bagasse and red mud for effective adsorption of tetracycline hydrochloride. *J. Environ. Chem. Eng.* **12**, 113041. https://doi.org/10.1016/j.jece113041 (2024).
46. Chen, L. et al. High adsorption of sulfamethoxazole by an amine-modified polystyrene-divinylbenzene resin and its mechanistic insight. *Environ. Sci. Technol.* **50**, 6b02846. https://doi.org/10.1021/acs.est6b02846 (2016).
47. Huang, D. et al. Nitrogen-doped nanocarbon derived from candle soot for persulfate activation on sulfamethoxazole removal: Performance and mechanism. *J. Colloid Interface Sci.* **629**, 121. https://doi.org/10.1016/j.jcis08.121 (2022).
48. Chen, Y. et al. Preparation of *Eucommia ulmoides* lignin-based high-performance biochar containing sulfonic group: Synergistic pyrolysis mechanism and tetracycline hydrochloride adsorption. *Bioresour. Technol.* **329**, 124856. https://doi.org/10.1016/j.biortech124856 (2021).
49. Yan, L. et al. Removal of tetracycline from water by adsorption with biochar: A review. *J. Water Process.* **60**, 105215. https://doi.org/10.1016/j.jwpe105215 (2024).
50. Brito, M. J. P. et al. Adsorption of the textile dye Dianix® royal blue CC onto carbons obtained from yellow mombin fruit stones and activated with KOH and H_3PO_4: Kinetics, adsorption equilibrium and thermodynamic studies. *Powder Technol.* **339**, 334–343. https://doi.org/10.1016/j.powtec.2018.08.017 (2018).
51. Mahdieh, M. M., Vahid, K., Vahab, G., Anis, A. & Mika, S. Adsorption isotherm models: A comprehensive and systematic review. *Sci. Total Environ.* **812**, 151334. https://doi.org/10.1016/j.scitotenv151334 (2021).
52. Yao, Q. et al. Adsorption of lead ions using a modified lignin hydrogel. *J. Polym. Res.* **465**, 10965. https://doi.org/10.1007/s10965-014-0465-9 (2014).
53. Cybelle, M. et al. Comparative and competitive adsorption of copper, lead, and nickel using chitosan immobilized on bentonite. *Carbohydr. Polym.* **83**, 528–536. https://doi.org/10.1016/j.carbpol.2010.08.013 (2011).
54. Yao, B. et al. Sustainable biochar/$MgFe_2O_4$ adsorbent for levofloxacin removal: Adsorption performances and mechanisms. *Bioresour. Technol.* **340**, 125698. https://doi.org/10.1016/j.biortech125698 (2021).
55. Zeng, Z. et al. Research on the sustainable efficacy of g-MoS_2 decorated biochar nanocomposites for removing tetracycline hydrochloride from antibiotic-polluted aqueous solution. *Sci. Total Environ.* https://doi.org/10.1016/j.scitotenv08.108 (2019).
56. Li, X. & Shi, J. Simultaneous adsorption of tetracycline, ammonium and phosphate from wastewater by iron and nitrogen modified biochar: Kinetics, isotherm, thermodynamic and mechanism. *Chemosphere* **293**, 133574. https://doi.org/10.1016/j.chemosphere133574 (2022).
57. Li, M. et al. Performance of magnetic graphene oxide/diethylenetriaminepentaacetic acid nanocomposite for the tetracycline and ciprofloxacin adsorption in single and binary systems. *J. Colloid Interface Sci.* **521**, 150–159. https://doi.org/10.1016/j.jcis.2018.03.003 (2018).
58. Yang, H. et al. Magnetic porous biochar as a renewable and highly effective adsorbent for the removal of tetracycline hydrochloride in water. *Environ. Sci. Pollut. Res.* **28**, 61513. https://doi.org/10.1007/s11356-021-15124-6 (2021).
59. Yang, Z. et al. Efficient activation of peroxydisulfate by modified red mud biochar derived from waste corn straw for levofloxacin degradation: Efficiencies and mechanisms. *J. Environ. Chem. Eng.* **11**, 111609. https://doi.org/10.1016/j.jece.111609 (2023).
60. Wu, Q., Muhammad, S. S. & Yu, W. Iron-nickel bimetallic metal-organic frameworks as bifunctional Fenton-like catalysts for enhanced adsorption and degradation of organic contaminants under visible light: Kinetics and mechanistic studies. *J. Hazard. Mater.* **401**, 123261. https://doi.org/10.1016/j.jhazmat123261 (2020).
61. Zhao, X. et al. Study on adsorption performance and mechanism of peanut hull derived magnetic biochar for removal of malachite green from water. *Mater. Res. Express* **10**, 095504. https://doi.org/10.1088/2053-1591/acf756 (2023).

62. Sun, M., Ma, Y., Yang, Y. & Zhu, X. Effect of iron impregnation ratio on the properties and adsorption of KOH activated biochar for removal of tetracycline and heavy metals. *Bioresour. Technol.* **380**, 129081. https://doi.org/10.1016/j.biortech129081 (2023).
63. Liu, S. et al. Spatial distribution of heavy metal contaminants: The effects of water-sediment regulation in the Henan section of the Yellow River. *Sci. Total Environ.* **892**, 164568. https://doi.org/10.1016/j.scitotenv164568 (2023).
64. Wang, Y., Xu, J. & Zhang, L. Watershed scale spatiotemporal nitrogen transport and source tracing using dual isotopes among surface water, sediments and groundwater in the Yiluo River Watershed, Middle of China. *Sci. Total Environ.* **833**, 155180. https://doi.org/10.1016/j.scitotenv155180 (2022).
65. Zhang, D., Yang, J., Huang, X., Liu, S. & Zhang, Z. Sources of dissolved heavy metals in river water of the Yiluo River basin based on sulfur isotope of sulfate. *China Environ. Sci.* **39**, 2549–2559. https://doi.org/10.19674/j.cnki.issn1000-6923.2019.0304 (2019).
66. Chen, Z. et al. Pollution, cumulative ecological risk and source apportionment of heavy metals in water bodies and river sediments near the Luanchuan molybdenum mining area in the Xiaoqinling Mountains China. *Mar. Pollut. Bull.* **205**, 116621. https://doi.org/10.1016/j.marpolbul.2024.116621 (2024).
67. Wang, Y. et al. Tetracycline removal from aqueous solution by magnetic biochar modified with different iron valences: A comparative study. *Sep. Purif. Technol.* **339**, 126614. https://doi.org/10.1016/j.seppur126614 (2024).
68. Xu, B. et al. Acid-modified red mud biochar for the degradation of tetracycline: Synergistic effect of adsorption and nonradical activation. *J. Environ. Manag.* **347**, 119077. https://doi.org/10.1016/j.jenvman119077 (2023).
69. Arun, K. V. et al. Biomass pyrolysis: A review on recent advancements and green hydrogen production. *Bioresour. Technol.* **364**, 128087. https://doi.org/10.1016/j.biortech.2022.128087 (2022).
70. Md, M. M., Ao, W., Xiao, L., Xiao, J. & Deng, S. Preparation of low-cost sludge-based highly porous biochar for efficient removal of refractory pollutants from agrochemical and pharmaceutical wastewater. *J. Hazard. Mater.* **478**, 135572. https://doi.org/10.1016/j.jhazmat.2024.135572 (2024).

Acknowledgements

This work was supported by Key Research and Development Special Project of Henan Province, China (251111321700), Henan Province Science and Technology Attack Plan Project (242102321069, 242102321076, 242102321119 and 242102320075), Key Scientific Research projects in Higher Education Institutions of Henan Province (24B610013, 24B610015), the Scientific Research Team Plan of Zhengzhou University of Aeronautics (23ZHTD01012) and Provincial Innovation and Entrepreneurship and Training Program for College Students (202410485047, 202410485011). This study was also supported by Zhengzhou Key Laboratory of Watershed Environmental Treatment and Zhengzhou Key Laboratory of Environmental Functional Materials.

Author contributions

X. Z.:conceptualization, design experiments,manuscript writing, B. Z.:conceptualization, design experiments,manuscript writing, Z. L.:results analysis, manuscript writing, Q. Z.:results analysis, M. Y.:results analysis, D. L.:investigation, results analysis, K. Z.:investigation, results analysis, X. W.:investigation, results analysis, H. Z.:investigation, results analysis.

Funding

Henan Province Science and Technology Attack Plan Project (242102321069, 242102321076, 242102321119, 242102320075 and 252102320129, 242102321069, 242102321076, 242102321119, 242102320075 and 252102320129, 242102321069, 242102321076, 242102321119, 242102320075 and 252102320129), Provincial Innovation and Entrepreneurship and Training Program for College Students (202410485047, 202410485011, 202410485047, 202410485011), Key Scientific Research projects in Higher Education Institutions of Henan Province (24B610013, 24B610015, 24B610013, 24B610015), the Scientific Research Team Plan of Zhengzhou University of Aeronautics (23ZHTD01012), Key Research and Development Special Project of Henan Province, China (251111321700).

Competing interests

The authors declare no competing interests.

Additional information

Correspondence and requests for materials should be addressed to X.Z. or B.Z.